COPY 1,

161 Cop

RD-74-24

AD/A-003 673

STUDY OF RUNWAY DEFORMATION CONTOURING USING HOLOGRAPHIC TECHNIQUES

C. G. Murphy

Science Applications, Incorporated

Prepared for:

Defense Nuclear Agency
Air Force Weapons Laboratory
Federal Aviation Administration

NAVAL
LIBRARY
SEP 25 '79

November 1974

DISTRIBUTED BY:

NTIS
National Technical Information Service
U. S. DEPARTMENT OF COMMERCE

UNCLASSIFIED

SECURITY CLASSIFICATION OF THIS PAGE (When Data Entered)

AD/A003 673

REPORT DOCUMENTATION PAGE

READ INSTRUCTIONS BEFORE COMPLETING FORM

1. REPORT NUMBER: AFWL-TR-73-282 and FAA-RD-74-24

2. GOVT ACCESSION NO.

3. RECIPIENT'S CATALOG NUMBER

4. TITLE (and Subtitle): STUDY OF RUNWAY DEFORMATION CONTOURING USING HOLOGRAPHIC TECHNIQUES

5. TYPE OF REPORT & PERIOD COVERED: Final Report, January 1973 - January 1974

6. PERFORMING ORG. REPORT NUMBER: SAI-73-510-AQ

7. AUTHOR(s): C. G. Murphy

8. CONTRACT OR GRANT NUMBER(s): DNA 001-73-C-0041

9. PERFORMING ORGANIZATION NAME AND ADDRESS: Science Applications, Inc, Albuquerque, New Mexico 87108

10. PROGRAM ELEMENT, PROJECT, TASK AREA & WORK UNIT NUMBERS: Program Element, Project 7310

11. CONTROLLING OFFICE NAME AND ADDRESS: Defense Nuclear Agency, Washington, DC 20305

12. REPORT DATE: November 1974

13. NUMBER OF PAGES: 130 - 131

14. MONITORING AGENCY NAME & ADDRESS (if different from Controlling Office): Air Force Weapons Laboratory, Kirtland Air Force Base, NM 87117

15. SECURITY CLASS. (of this report): UNCLASSIFIED

15a. DECLASSIFICATION/DOWNGRADING SCHEDULE

16. DISTRIBUTION STATEMENT (of this Report): Approved for public release; distribution unlimited.

17. DISTRIBUTION STATEMENT (of the abstract entered in Block 20, if different from Report): Same as block 16.

Reproduced by NATIONAL TECHNICAL INFORMATION SERVICE, US Department of Commerce, Springfield, VA. 22151

18. SUPPLEMENTARY NOTES

This research was performed under DNA Contract DNA 001-73-C-0041. Funds to DNA were provided by AFWL MIPR FY3592-74-10059. FAA funds were provided by FAA Interagency Agreement FA-73-WAI-361.

19. KEY WORDS (Continue on reverse side if necessary and identify by block number)

airfield pavement deformation
holography
pavement deflections
civil engineering
interferometry
deformation contouring

20. ABSTRACT (Continue on reverse side if necessary and identify by block number)

This work is designed to show that the modern optics methods of holography and moire for deformation measurements are applicable in the field. The holographic methods described are general holography, holographic interferometry by double exposure, live fringe and constant amplitude vibration, holographic contouring by the dual frequency, dual-source and dual-index methods. Moire methods of producing contours for topology and deformations are described which use the holographic contouring and grid projection techniques. (OVER)

DD FORM 1 JAN 73 1473 EDITION OF 1 NOV 65 IS OBSOLETE

UNCLASSIFIED

SECURITY CLASSIFICATION OF THIS PAGE (When Data Entered)

ABSTRACT (Cont'd)

Experimental techniques are given for each of these methods and the suitability of each for field use is evaluated in terms of key parameters. Two laboratory experiments are presented to demonstrate the technologies involved in holographic and moire deformation contouring. The moire method using a coherent projected grid was chosen as the optimum one for producing runway deformations because of its simpler technology and correct deformation measuring range. The feasibility of this moire method is shown by considering the areas of importance in measuring a whole field deformation pattern that is typical of deformation basins measured by some existing techniques. Recommendations for a modular approach to producing a deformation contouring device are given.

CONTENTS

Section		Page
I	INTRODUCTION	1
II	DEFORMATION CONTOUR GENERATION: METHODS	3
	1. Stereo Pair Imaging	4
	2. Holographic Surface Recording	4
	3. Moire Deformation Contours	5
III	DEFORMATION CONTOUR GENERATION: EXPERIMENTAL TECHNIQUES	7
	1. Holography	7
	2. Moire	14
	a. Holographic Contouring for Moire Grids	14
	b. Projected-Grid Moire	19
IV	DEFORMATION CONTOUR GENERATION: EXPERIMENTAL RESULTS	38
	1. General Experimental Consideration	38
	2. Projected-Grid Moire Experiment	38
	3. Dual-Wavelength Holographic Contouring Experiment	54
	4. Evaluation of Experimental Results	60
V	CONCLUSIONS AND RECOMMENDATIONS	63
	1. Choice of Alternative Methods	63
	2. Example System Engineering	64
	3. Feasibility Conclusions	72
	a. Feasibility	72
	b. Compatibility with Transfer Function Techniques	73
	c. Suggestions for Further Development	74
	APPENDIX A HOLOGRAPHY	79
	APPENDIX B HOLOGRAPHIC INTERFEROMETRY	83
	APPENDIX C MOIRE FRINGES	90
	APPENDIX D TOPOLOGY AND DEFORMATION CONTOURING BY MOIRE FRINGES	96
	APPENDIX E HOLOGRAPHIC CONTOURING	104
	APPENDIX F PROJECTED-MOIRE GRID SENSITIVITY	107
	BIBLIOGRAPHY	115

ILLUSTRATIONS

Figure		Page
1	Typical Holographic Arrangement	8
2	Geometry for Holography of Large Surface	12
3	Resolution Range of Deformation Contouring Methods	37
4	Moire Grid Deformation Contouring Arrangement	40
5	Detail of Coherent Grid Projector	41
6a	Single-Disk Moire Deformation Contours	45
6b	Double-Disk Moire Deformation Contours	46
6c	Four-Disk Moire Deformation Contours	47
6d	Eight-Disk Moire Deformation Contours	48
7a	Deformation Due to Single-Disk Load	50
7b	Deformation Due to Dual-Disk Load	51
7c	Deformation Due to Four-Disk Load	52
7d	Deformation Due to Eight-Disk Load	53
8a	Double-Disk Moire Deformation Contours with Increased Load	55
8b	Increased Load Dual-Disk Deformation	56
9	Dual-Wavelength Holographic Contouring Arrangement	57
10	Contour Lines Produced by Ruby Laser Operating at Two Wavelengths	61
11	Development and Use Flow Chart	76
12	Basic Terms for Holography	80
13	Moire from Two Gratings of Different Pitches	94
14	Moire Between Two Gratings at Angle to Each Other: Imperfections Cause Jagged Appearance in Fringes	95

ILLUSTRATIONS (CONT'D)

Figure		Page
15	Geometry Showing Change in x, Δx Due to Change in z	98
16	Three-Dimensional Moire Analysis Geometry	109
17	Moire Analysis Angle Detail	111
18	Spherical Angles for Finding Angle between Two Vectors	112
19	Geometry to Determine Angles	113

TABLES

Table		Page
1	Key Parameters--Double-Exposure Holographic Interferometry	28
2	Key Parameters--Live Fringe Holographic Interferometry	30
3	Key Parameters--Constant Amplitude Vibration Holographic Interferometry	32
4	Key Parameters--Dual-Frequency Holographic Contouring	33
5	Key Parameters--Shadow Grid Moire Contouring	34
6	Key Parameters--Incoherent Projected Grid	35
7	Coherent Projected Grid	36

LIST OF SYMBOLS

$\Delta\phi$	phase change introduced by deformation
$J_o(x)$	Bessel Function with argument x
λ	wavelength of light
ℓ_o	coherence length of laser
a	distance from light source to pavement
b	radius of illuminated area on pavement
p	spatial frequency or pitch
E	energy required for hologram exposure
ν	angle between illumination and reference beams
ρ	reflectivity of pavement
c	laser output energy during exposure
r	reference to scene intensity ratio at hologram plate
δ	contour fringe spacing or interval
$\eta_{1,2}$	indices of refraction for medial 1 and 2
d	separation distance of planes of light
θ	angle between two combining beams of light
ϕ	angle between normal to pavement and line to observation point
Φ	angle between normal to light planes and the line to the observation point
X	grid spacing
Λ	lens diameter
D	distance from camera to object
ΔD	depth of focus
S	characteristic laser speckle size

LIST OF SYMBOLS (CONT'D)

N	ratio of grid spacing to speckle size
$\hat{s}$	unit vector along perpendicular between light planes from point to be analyzed
$\hat{v}$	unit vector toward observer from point to be analyzed
s	optical path
$\Delta\ell$	difference in distances to camera from portion of runway, in view
T	temperature
$\frac{\partial n}{\partial T}$	change in index of refraction with change in temperature
v	specific volume
^{o}K	degrees Kelvin
B	isobaric thermal expansivity
t	amplitude transmittance
$Re^{i\phi_r}$	reference beam complex amplitude
$Oe^{i\phi_o}$	object complex amplitude
I	intensity
t_b	portion of transmittance without phase factors
C	proportionality constant
A_p	complex amplitude behind the plate
A_o	complex amplitude of light traveling in the direction of the original object wave
$A_{1,2}$	reconstructed complex amplitude from exposure 1 or 2
I_o	intensity observed in original object wave direction

LIST OF SYMBOLS (CONT'D)

θ_i	angle between normal to surface and illumination beam
θ_s	angle between surface normal and line to observer
O	order defined to be an integer where destructive interference occurs
Λ	deformation of runway surface
τ	time variable
P	period of oscillation
ϕ_o	phase shift
ω	frequency
L, L_o	period of grating
x	position variable in pavement surface plane
γ	angle of rotation of grid
ξ	position normal to light planes
p_o	pitch along direction normal to wavefront
α	angle between normal to surface and the line to the light plane source
β	angle between normal to surface and line to observer
a_1, b_1, b_2	angles used in showing trig identities
Δb	difference in angles b_1 and b_2
K, K'	proportionality factors
Δx	shift in grid line due to deformation
z	position variable in direction normal to pavement surface
Δz	deformation of surface along z
$\Lambda(x,y)$	acoustical amplitude distribution of surface vibration

LIST OF SYMBOLS (CONT'D)

A_R	complex amplitude of light in reference beam
$\hat{n}$	unit vector normal to surface from point to be analyzed
$\hat{t}$	unit vector toward the grid projection source from the point to be analyzed
V	observer position with components V_x, V_y, V_z
T	source position with components T_x, T_y, T_z
Ω	angle between $\hat{n}$ and $\hat{s}$
θ_v	angle between line to observer and x coordinate in the pavement surface plane
θt	angle between line to source and x coordinate in the pavement surface plane
ΔO	change in fringe order

SECTION 1

INTRODUCTION

The feasibility of holographic and moire contouring methods is determined for measuring deformation basins of aircraft runways. Deformation basins are used in determining runway time to failure, prediction of failure locations, and for calculating pavement deformation using transfer function modeling. Present methods of determining runway basins involve the use of devices buried in the runway at predetermined points. The difficulties in making this measurement and the data transformations necessary for reference frame conversion to the road frame of reference introduce errors that limit the utility of transfer function modeling of runways. Also, the holes introduced into the runway for instrumentation placement may cause acceleration of runway failure mechanisms and alter the actual transfer function as compared to the undisturbed runways. The noncontact and area coverage provided by optical techniques provides for an obvious solution to these problems. The area coverage provides data points which may be selected in the prime-mover reference system and allow greater freedom in selection of data points for input to transfer function codes. An optical system may also be moved to provide data at any location on the airfield or can be carried on the aircraft or other heavy load vehicle. It also can be used in preventative maintenance by repeated scanning of high stress regions. Of course, the noncontact aspect provides for no effect of the measurement system on deformation data.

An additional reason for exploring these techniques is that the potential for applications in other areas is large. Recently developed technologies in the laser optics field have already found several uses in civil engineering metrology. Also, laboratory methods of measuring deformation for nondestructive testing can now be applied in the field to pavements research. Among these new applications which might continue from the development of an optical deformation contouring system are thermal cycle, creep, and vibration measurements that would yield valuable data for use in preventing and predicting pavement failure.

The introduction of coherent optical techniques to the civil engineer should also yield new requirements and applications. For instance, the high sensitivity measurement of linear voltage differential transducer (LVDT) deflection gages is offset by their deterioration with time. An optical solution to this problem is the use of the diffractogage, a sensitive deformation detector which has proven, very long-term reliability under adverse environmental conditions. Another example is the technique of surface-wave detection of waves with amplitude sensitivity of a few angstroms by laser scattering techniques. Beginning with one coherent optical system, the typical reluctance to try new techniques is overcome and further advances in technology can occur.

SECTION II

DEFORMATION CONTOUR GENERATION: METHODS

In this section we describe various methods of making deformation contours. We limit our discussion to whole-field coverage methods because of the advantages of the parallel input providing data redundancy and identification of anomalous points. Also, the external noncontact nature of area detection allows for compensation for environmental effects on the instrument. Point-by-point techniques can give excellent accuracy at a given point and a continuous time history but require complex and time-consuming operations on the runway. The area coverage techniques transfer the effort to the laboratory and computer, thus saving time in the field.

In order to produce deformation contours, it is required that the load-free surface topology be stored and then compared to the loaded surface. Therefore, any method of recording the surface topology is a candidate for implementation as a deformation basin detector and should be considered until shown to be impractical. The parameters of a topology recorder which are pertinent to deformation measurement are sensitivity, range, repeatibility, area of measurement, ease of implementation, rates of data gathering, advances in state-of-art required for runway use, and compatibility with present pavement evaluation research. The methods discussed here range in sensitivity from stereo-pair contouring to holographic interferometry.

1. Stereo-Pair Imaging

Stereo-pair imagery can be used to produce contour maps by the standard methods of observing depths in a stereo viewer. By making contours before and after deformation, the technique could be used to detect gross changes in the surface. The stereo-pair method is applicable to contouring mountains, craters, and objects with fairly large changes in depth compared to the area under view. Unfortunately, the contours are subject to errors in depth judgement and deformation observations would be unreliable and insensitive because the contour line spacing is too large for deformation detection on runways. The precision is reduced by the human judgement of the depth. The best sensitivity that could be expected is to determine deformation of the order of inches.

2. Holographic Surface Recording

The most sensitive method of topology recording is holography. The holographic technique records the light wavefront from the scene in both amplitude and phase. Details are given in Appendix A. When this wavefront is reconstructed, the image perceived by the observer is three dimensional in nature and even the microstructure of the object is presented to wavelength of light precision. Coherent speckle is present and must be kept smaller than the sensitivity required in the measurement. Once the surface topology has been recorded, various methods

exist which can use the reconstructed wavefront; the stereo-pair technique could even be used. The most sensitive method of application is called holographic interferometry. Several types of holographic interferometry exist. Among them are double-exposure and live-fringe interferometry which are discussed in detail in Appendix B. These techniques give images of the object which is modulated by a cos $\Delta\phi$ term. The phase change, $\Delta\phi$, introduced by the deformation produces dark or light areas in the image of the object which can be analyzed by using the optical path difference to relate the deformation and the observed phase change. Also, the technique of constant amplitude holographic interferometry for vibrating surfaces is given in Appendix B. In this case the image is modulated by a $J_0^2(x)$ function, where $J_0(x)$ is the first-order Bessel function.

3. Moire Deformation Contours

We have discussed two methods of determining the deformation of a surface, stereo-pair contouring and holographic interferometry. The first is a gross method where the deformation is taken by comparing two contours. The second involves the light intensity transmitted by a holographic plate and uses the modulation of the image as the indicator of the deformation. If we combine the approaches and provide contour maps by one of many techniques and then use the contour map as a filter, we obtain an image of the object modulated by dark and light

regions called fringes. This technique is called moire fringe deformation measurement. The applications of the moire method for through transmission and specular reflection deformation measurements are numerous. Applications to contouring and deformation measurement of diffuse surfaces are less numerous but modern optical techniques are making these applications feasible. A discussion of the moire fringe and a derivation of the intensities that produce the fringes is given in Appendix C.

A simple explanation of moire fringes is that two sets of parallel lines whose spacings vary slightly will line up in some areas and not in others. Where the lines are in alignment, light is transmitted in one-half the area. Where the lines are fully misaligned, the light is blocked. The visibility is limited in this simple case, but the method is valuable because the sensitivity can be varied with the choice of line spacing. To produce surface topology contours, lines are projected on the object and compared to a uniformly spaced master. To produce deformation contours, the lines projected into the undeformed surface are used as a master and the lines projected on the deformed surface are compared with it. The sensitivity is approximately one line spacing but varies with projection and viewing geometry. The analyses for topology and deformation analysis are given in Appendix D where moire contouring is discussed in detail. Also given there are discussions of comparison of similarly shaped objects and of constant amplitude vibration measurement by moire methods.

SECTION III

DEFORMATION CONTOUR GENERATION: EXPERIMENTAL TECHNIQUES

We have briefly described the methods of producing topology and deformation contours and have given analyses to show how the images of scenes are modulated by fringes which represent these contours. We now give experimental techniques used to implement the various contour methods. The methods discussed are the double exposure, live fringe and constant amplitude vibration methods of holographic interferometry and the methods of producing grid lines on the object for the moire. These moire methods use grids produced by holographic contour methods: dual frequency, dual source, dual index, and grid-projection methods: grid shadow, ordinary projection, and coherent projection.

1. Holography

The equipment used in holography consists of a coherent source, a beam splitter, mirrors, beam expanding lenses, spatial filters, and a holographic plate. If the coherent source is continuous rather than pulsed, there must be vibration isolation to keep motion of the components to a minimum. The arrangement given in Figure 1 shows a typical arrangement for diffuse object holography. As we discussed earlier, double exposure interferometry is performed by making two exposures on the same hologram while live fringe interferometry is performed by making a hologram, developing the plate, and

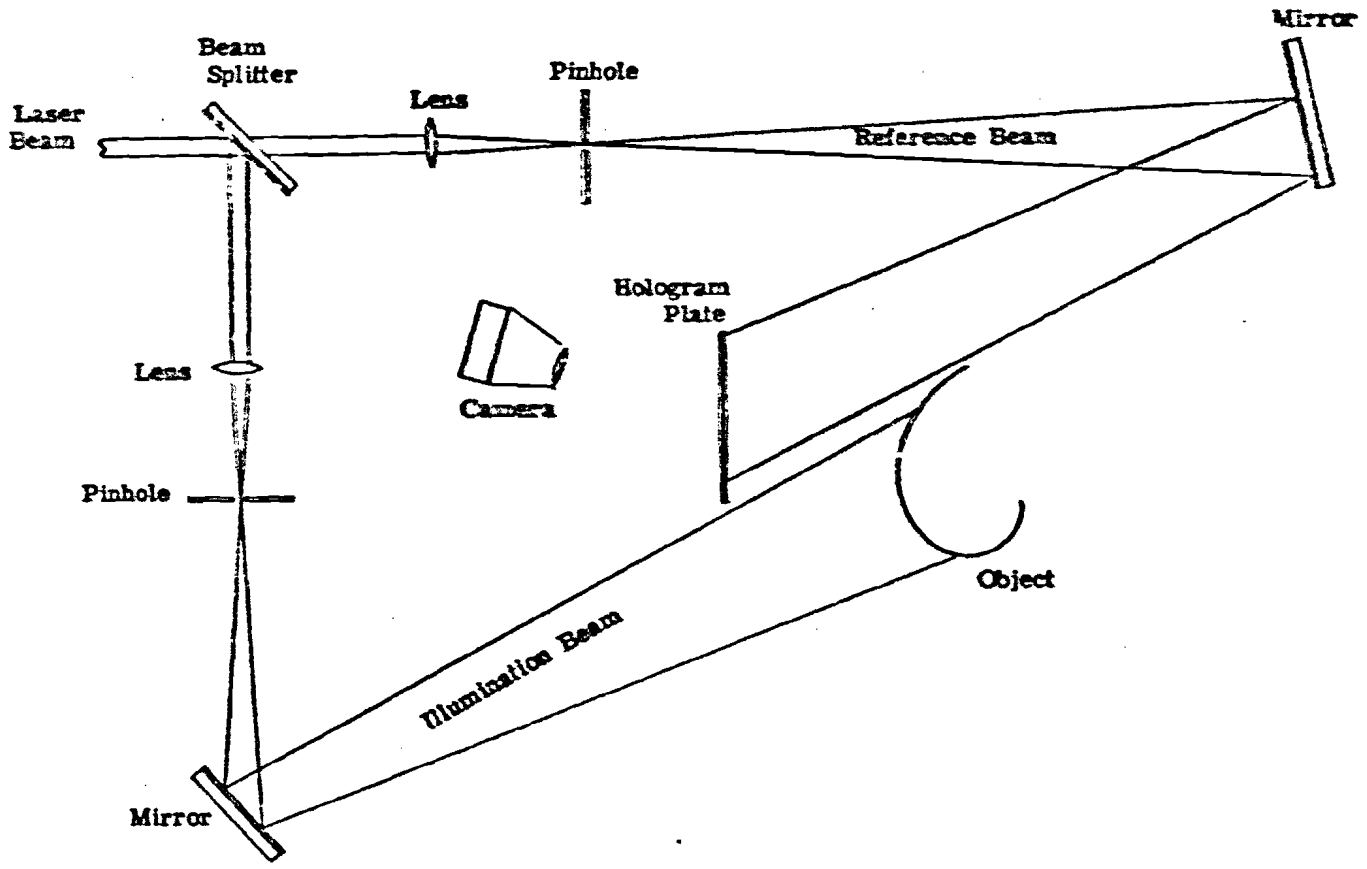

Figure 1. Typical Holographic Arrangement.

replacing it in the holder. By re-illuminating the object and reconstructing the hologram simultaneously, the deformations of the object show up as fringes on the object image. Constant amplitude vibration can be detected by a single exposure which integrates many vibration cycles or by live fringe methods. Most of the discussion here holds for all these methods.

The arrangement given in Figure 1 has several details which should be noted. First, the length of the object illumination beam is as close as possible to being equal to the reference beam length. The region in space where the path lengths differ by less than the coherence length is the region that is reconstructed by holography. Therefore, the paths are adjusted so that a hologram can be made in the proper scene region. Second, the hologram plate is located so that its normal bisects the angle between the line from object to plate and the line of the reference beam. This is required to ensure that the most efficient hologram is produced since holographic diffraction is in reality a Bragg process where volume effects in the holographic emulsion are important. Third, the angle between the object-to-plate and reference beam is optimized to yield comfortable viewing away from the reference beam, but a minimum angle is required to reduce the film resolution requirements. Fourth, unless the laser is a pulsed type and can stop-motion any vibration, the table on which the arrangement stands must be vibration isolated and protected from strong air currents. No component motion greater than about $\lambda/8$ can be allowed during the hologram

exposure. Also, the ratio of the intensity of the reference beam to the intensity scattered from the object is controlled to obtain either the optimum hologram or the highest visibility fringes. Finally, the application of stress or vibration to induce deformation of the object is controlled so that body motions are minimized. If the experiment is a live fringe one, the hologram plate is usually surrounded by a wet tank or in-place developer to reduce the effects of emulsion shrinkage induced by the development process. Exposure and development of the plate are carefully controlled to achieve the optimum hologram. In some cases the hologram is bleached to enhance the efficiency and obtain brighter holograms.

When reconstruction is performed, a camera is used to record the fringe system. This step is not as straightforward as it sounds because the fringes are localized (have their highest visibility) in a place other than on the object, and a large depth of field is required to have both the object and fringes in clear focus. This is not a problem in double-exposure interferometry where both deformed and undeformed images are affected the same by emulsion effects. However, the emulsion shrinkage causes severe displacement of the fringe localization in live fringe interferometry. Also, the reconstruction beam must have exactly the same wavefront as the original reference beam if aberrations are to be minimized. This means that the plate must be replaced to accuracies of

better than one wavelength if error-free fringe analysis is to be made in live-fringe interferometry.

The above makes holographic use outside the laboratory seem foreboding, but successful quantitative holographic interferometry has been performed by this author in severe environments. With the use of pulsed laser sources, reference points in the scene, and Fourier optics techniques to reduce noise, the use of holography in severe environments is now possible. The following are some evaluations of the three types of holographic interferometry as applied out of the laboratory in a field situation.

In field applications of holography several considerations must be made to insure data over a given area. We will discuss these using a simple example given in Figure 2. The first point to consider is coherence length, ℓ_o. The maximum difference is reference path, and illumination path is

$$\Delta\ell = 2\left(\sqrt{a^2 + b^2} - a\right)$$

and for holography we must have

$$\Delta\ell < \ell_o$$

where ℓ_o is the coherence length. The maximum spatial frequency response of the hologram plate, p_{max}, is related to the minimum energy for hologram exposure, E_{min}, by the empirical relation

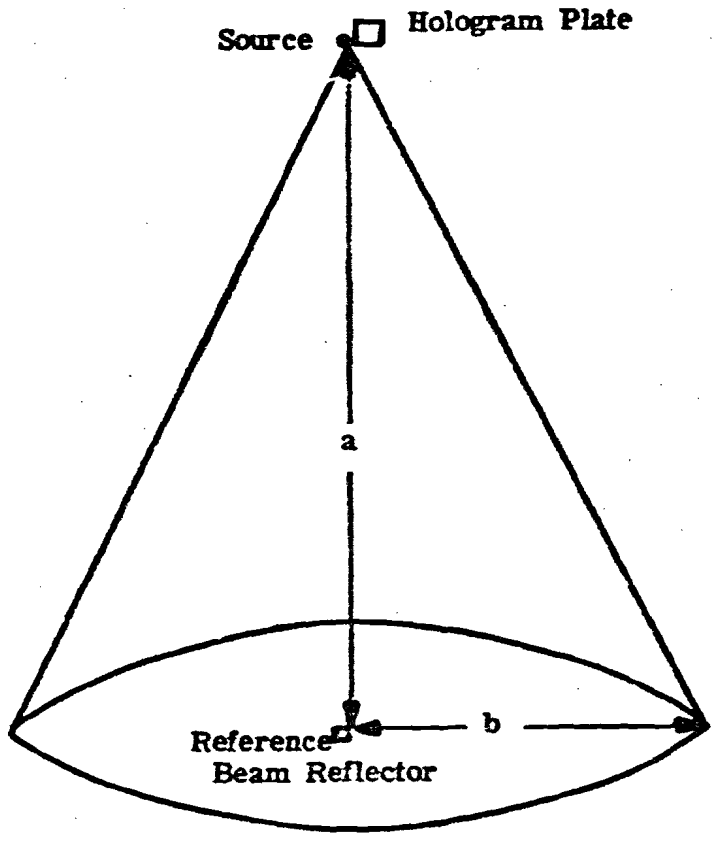

Figure 2. Geometry for Holography of Large Surface.

$$p_{max} = K \log E_{min}$$

where K is a constant which depends on the exposure time. Therefore, both the maximum frequency response and the minimum energy required for exposure at that frequency must be considered.

The spatial frequency required to produce a hologram is given by:

$$p = \frac{2 \sin \nu/2}{\lambda}$$

where λ is the wavelength and ν is the angle between the illumination and the reference beam. For our example

$$p = \frac{1}{\lambda}\left[2\left(1 - \frac{a}{\sqrt{a^2 + b^2}}\right)\right]^{\frac{1}{2}}$$

gives the maximum spatial frequency that is expected from the arrangement. The energy per unit area returned to the plate from the illuminated region is

$$E = \frac{\rho}{(r + 1)} \frac{\epsilon}{(a^2 + b^2)}$$

where r is the reference to scene intensity ratio, ρ is the reflectivity, and ϵ is the total laser energy emitted during

the exposure. With these equations and a given geometry, a and b, we can find the approximate maximum spatial frequency by using a wavelength of 500 nm. This ensures a factor of safety. Then, the film is chosen by considering those available with response at that spatial frequency. Finally, the total laser energy required for exposure is found by using the surface reflectivity, the beam ratio, and the minimum exposure energy from the film specification. These equations could also be used to predict the geometries and surface which can be hologramed for a given laser and film.

The beam ratio required in a given situation depends on the desired results. Recommended reference to scene ratios for imaging are about 4, but the best fringe visibility is obtained at ratios from 1 to 1.5 depending on surface reflectivity. Surfaces with high reflectivity require closer to 1:1 ratios of reference to scene intensity.

2. Moire

a. Holographic Contouring for Moire Grids

The methods of holographic contouring require the same holographic steps as the deformation holographic interferometry, but the hologram process is changed so that topology contours are obtained instead of deformation contours. These can be used in a moire form to obtain less sensitive deformation contours. There are three well-developed holographic contouring methods: dual wavelength, dual index, and dual source.

The method of dual wavelength can be explained in simple terms by the observation that if a source is operating at two different temporal frequencies these frequencies will beat together and cause the output to vary with time with several frequency component terms, one of which is the difference frequency. With optical sources this difference frequency is the only observed frequency since other terms oscillate too fast to be detected. The appearance is that of a light beam with variations in time. Given a holographic arrangement, the light path for the scene beam varies with object depth while the reference beam has fixed length. When the scene and reference beams are brought together at the hologram plate, they vary in phase due to the differences in the path lengths caused by the varying scene depth. When the time variations are in phase, a hologram image is produced but out-of-phase signals produce no hologram. Thus, the scene hologram exists only at those distances where the time signals are in phase and the scene is modulated by contour fringes. This explanation is a simplified one, and an alternative analysis is derived in Appendix E where the equation for contour fringe levels is found to be

$$\delta = \frac{\lambda_1 \lambda_2}{2|\lambda_2 - \lambda_1|}$$

where δ is the separation distance of the contour fringes and $\lambda_{1,2}$ are the two wavelengths. Additional details on reconstruction of dual-frequency holograms are given in Appendix E.

One difficulty with this method is the limited number of sources with dual-wavelengths and holographic coherence. Dual-wavelength operation of pulsed ruby lasers is possible by the selection of double laser modes using an etalon in the optical laser cavity. Experimental results of such an experiment are given in Section IV. Other feasible alternatives are the argon-ion laser which operates at many strong wavelengths. Its two strongest wavelengths are 515 nm and 488 nm. The contour fringe spacing for this laser would be 4.7 μm (~0.2 thousandths of an inch). However, wavelength tuning of the sensitivity is not possible. The He-Cd laser also operates at several fixed wavelengths.

The usual difficulties for holography also are present and the promising sensitivity of the argon-ion laser must be considered in light of its continuous wave operation. Pulsed-mode operation is possible for these lasers, but operation with long coherence lengths in these modes is not common practice. Also, the single exposure required presents an advantage of contouring by this method.

If laser modulators existed so that the time variations were externally induced, it would be ideal. Not only would sensitivities be variable, but the shape of the pulses could be varied from sinusoidal to obtain narrow contour lines on a bright object or other interesting variations. Modulators do not exist at this time for this type of operation but may in the future because of the demand for fulfilling the use of the information-carrying capability of the laser beam.

Dual-index contouring by holography requires the immersion of the object to be contoured into two fluids of varying index for two exposures. The explanation for this technique is similar to that of dual wavelength contouring except that the key advantage of holography is used; that is, the surface topology at one time is stored for interferometric comparison at another time. By changing the index of the fluid surrounding the object, the effective wavelength is changed to

$$\lambda_1 = n_1 \lambda_o$$

where λ_1 is the new wavelength and n_1 is the index of refraction. When we compare the two images by reconstruction of the double-exposure hologram, we have simulated the process of dual-wavelength contouring with the fringe separation representing contours of depth,

$$\delta = \frac{\lambda}{2} \frac{1}{|n_2 - n_1|}$$

which can be obtained by substituting λ/n_1 for λ_1 and λ/n_2 for λ_2 in the dual-wavelength contour depth relationship.

Although the immersion method is not very useful outside the laboratory, it does point out that double exposure techniques are subject to errors if index variations are present between exposures.

The third holographic contouring method is the dual-source technique which is achieved by a double exposure where the illumination source is moved between exposures. This method is an application which is equivalent to illuminating the scene with two different sources at the same time, but the time storage advantage of holography is used so that a single source can be used as both sources. For most field applications it is technically simpler to provide dual sources and make a single exposure so the techniques of coherent grid projection apply to dual source holographic contouring. By Thompson's Rule--holography should not be used when conventional techniques work--this method is redundant and adds unnecessary complexity unless single sources are required for other reasons.

These methods of holographic contouring provide topology maps that can be used to make deformation contours by their superposition, one map being made before the deformation and the other map being made after the deformation. The best contour reference (point which is equidistance from the contours) is to the side of the observer when deformation moire is to be used. This will make modifications to the usual analyses given for dual-index contouring but none for dual frequency or dual source since they can be applied with the reference point in various positions. Dual index is used only with the reference nearly in line with the observer, but the high sensitivity of dual-index method gives the type of topology maps required

for moire when angles between the surface normal and the observer are changed by only a few degrees from normal.

b. Projected-Grid Moire

Contouring of surfaces for use in moire deformation contouring can also be achieved by the projection of grid lines on the scene. The projection can be made by placing a screen near the object so that its shadow provides a surface grid while the screen acts as a reference grid. Also, a simple projector may be used to project a grid on the scene. Finally, the projector equivalent of the dual-source holographic contouring method can be used. For this case two coherent sources interfere and form a grid structure on the surface.

The shadow-grid method offers the advantage of being simple to implement for small objects. All that is required is a light source, a grid made up of black strings held on a frame, and a camera to record the moire between the grid and its shadow. Since no coherent light is used, laser speckle and coherent noise are not present. Resolution of this method is approximately the spacing of the grid. The main limitation is the construction of a grid, which covers the entire scene area and is sufficiently rigid to hold its shape accurately, and the closeness of the grid to the object. Also, higher-order frequencies sometimes beat together and cause aliasing on the scene. Aliasing appears as additional moire fringes. Motion

of the grid during exposure does not affect the contours and has the benefit of reducing the aliasing. The most serious disadvantage is the contour reference location directly above the plane of the grid. In order to record two topology contours which produce deformation contours, the reference should be to the side of the observer. This could be corrected by tilting the grid but then the limited depth of sharp shadows causes decreased fringe visibility. It may be possible to build a grid structure which is composed of many tilted grid segments which would work. This would be called a Fresnel grid since it would work on the similar principle of the Fresnel lens where segmented parts are used to obtain a large phase shift over an area while using only thin sheets.

One interesting alternative of this method is to use a large plastic grid instead of an opaque element grid. The intensity of light in the contour fringe is much higher since only the surface of the scene absorbs intensity.

The use of an ordinary projector which focuses a Ronchi ruling upon the scene is a viable one if the scene is of limited depth. The consideration of depth of focus of the projector also requires that the grid projector be directly above the scene. Special optics could be obtained which gave a tilted projection focal plane but the reference point is still fixed and does not have versatility for other applications. For viewing, grid cameras which perform tilted plane imagery are feasible because of the reduction in size obtained in photography.

They are called holosymmetrical optical systems and are not necessarily expensive or complicated and may be adjusted on the field. The projector system offers the advantage that no screen is located near the scene and no coherent noise or speckle is present in the image.

If a topology contour is required, a Ronchi ruling is used as a reference grid. However, it is not necessary for deformation contouring since the photograph of the projected grid on the object is to be compared with another grid projected on the deformed surface. The moire comparison is made as discussed in Appendix C and Appendix D.

Similar results may be obtained by the coherent grid projector except that no focal depth in the projector need be considered. The coherent grid projector works by the wavefront division of amplitude performed by a beamsplitter or by wavefront separation by mirrors. By separating the beam and recombining at an angle, the two beams interfere and produce an interference pattern. There are planes of light projected out from the device which appear as a grid whenever they strike the scene. Since the angles of the recombining beams can be controlled, the coherence length requirements are low.

The planes of light are separated by a distance

$$d = \frac{\lambda}{2 \sin \theta/2}$$

where θ is the angle between the two combining beams of light and λ is the wavelength. Since the rotation of optical components is a minor task, the variability of the angle and sensitivity is a prime advantage of this method. The achievement of a given resolution is obtained by placing a Ronchi ruling and the projected fringes to give an accurate scene pitch. The coherent projection method contours best when the contour reference plane is to the side of the observer. This enhances the use of the technique for deformation contour measurement. One disadvantage is that shadows and vignetting occur if large depressions or peaks occur in the scene. The contour interval is

$$\delta = (d/\cos \Phi)\cos \phi$$

where ϕ is the angle between the surface normal and the observer, d is the separation of the planes of light, and Φ is the angle between the normal to that plane and the viewing direction. This case holds only for a given point since for some optical arrangement the angles θ, ϕ, and Φ vary with position on the scene. Note that the arrangement has its highest sensitivity when the angle Φ is near zero. This is the case when the light planes come in from the side at 90°. Also, the sensitivity is nil if the observer is in line with the light planes. A detailed three-dimensional analysis of projected grid moire sensitivity is given in Appendix F.

The maximum subject size is limited by the ability of the camera to resolve the grid on the scene because the object either presents too large an area or because the scene has large depth variation. In either case the limitations is the depth-of-focus oi the camera. The discussion given earlier for the holographic application holds here except that the film resolution requirements are lessened. The depth of focus is given by

$$\Delta D = \frac{2XDA}{A^2 + X^2}$$

where X is the apparent grid spacing, A is the lens diameter, and D is the distance from the camera to the object. For resolution by the eye, X should not exceed the magnification times 0.003; however, cameras do not have the same limitation and X should be less than the maximum spatial frequency where film response is obtained times the magnification. Since $X << A$ in most cases,

$$\Delta D = \frac{2XD}{A}$$

Laser speckle is characterized by a size, S, equal to the Airy disk diameter

$$S \approx \frac{\lambda D}{A}$$

If we require the speckle to be smaller than the grid spacing by a factor of N, we obtain

$$\chi = N \cdot S$$

The focal depth can be found in terms of the speckle size using $S/\lambda = D/A$.

$$\Delta D \approx \frac{2\chi^2}{N\lambda}$$

A reasonable value of N is 5, so for a grid spacing of 0.1 mm and wavelength 0.5 nm we can have a depth-of-field

$$\Delta D \approx 0.1 \text{ meter}$$

Notice that this result turned out to be independent of the camera lens diameter and the camera distance. The dependence of the depth-of-field on the square of the grid spacing indicates that factors of two changes in sensitivity yield factor of four changes in depth-of-field. Also, the ratio of grid spacing to speckle size used here is only a reasonable guess as to the difference in speckle and resolution. The effect of exceeding the basic limitations in depth-of-focus will be an increase in

laser speckle which will only reduce the fringe visibility, not destroy the data completely.

The implementation of this technique is relatively simple since most types of standard interferometers may be used to make a projection of two beams at different angles. The double-exposure moire or the filter-comparison moire, discussed in Appendix D, can be used to produce the deformation moire. A constraint on the method is that the planes of light must remain stationary in some directions during the exposure. A motion of one-half the spacing during exposure can eliminate them completely if the motion is normal to the planes. However, one method of speckle removal is the motion of the source; and if motion were achieved in the direction of the light planes, no effect could be observed by the camera except speckle would be removed.

Both live fringe, double exposure and separate exposures could be used with this technique. Vibration detection is possible with this technique since time averaging over several cycles yields nodal patterns.

Since the method uses coherent sources, the stop-motion application of pulsed lasers is possible and fast moving deformations can be detected and measured. This is one of its advantages over ordinary projectors since no short time pulsed projectors exist in the few nanosecond range. Another advantage is the sine wave nature of interference of two sources. Other moire analyses ignore the square-wave grid structure

and assume that extra terms from the square wave are insignificant. A more accurate development would show the existence of aliasing and other errors. The coherent projected grid is sine wave inherently and none of these additional error terms are present.

We will now attempt to make a general comparison of the techniques of deformation contour generation before comparing the method for the specific application of deformation of runway pavements. Many statements have already been made on the details of application of the various techniques and an attempt is made to summarize them here by using tables and graphic displays.

This graphic form is simplifying, and dependences on other parameters are hidden. Therefore, the values and judgements are not absolute but are chosen to be self-consistent. For instance, if an improvement in one parameter is required, it may be possible with a sacrifice in other parameters. The values given here are those obtainable without large sacrifices in the general parameters of the method.

Tables 1 through 7 give key parameters for each of the methods of making whole field measurements and deformation contours of surfaces. The bar chart in Figure 3 gives a presentation of a key parameter, the range of sensitivities possible, for each of the techniques. The most desirable method would be one which has the sensitivity required but is not over sensitive so as to make positioning for comparison

difficult. The dual-frequency holographic contouring, shadow-grid moire, and projected-grid moire have the largest ranges with their minimum sensitivities in the 10 to 100 millimeter region. Also, the shadow-grid moire and the projected-grid moire can be used at varying sensitivities so that the sensitivity is not made smaller than necessary.

Table 1

KEY PARAMETERS--DOUBLE-EXPOSURE HOLOGRAPHIC INTERFEROMETRY

Item	Data
Wavelength (λ)	pulsed-694 nm; continuous-633 nm; 515 nm; 488 nm
Minimum Resolution	$\lambda/8$ interpolation to 1/4 fringe
Range	λ to 25λ minimum based on sufficient fringe to interpolate maximum based on 50 fringes in scene
Repeatability	$\lambda/2$ due to body motion error (could be reduced if reference is in scene)
Direction of Deformation	all least sensitive in direction out of plane of reference beam and illumination beam
Noise (speckle)	low uses large aperture in recording camera
Noise (coherent)	pulsed-fair; continuous-good
Scene Distortion	low < ±.01% in literature with special handling < ±1% with routine handling
Fringe Visibility	near 1 coherence length must be long compared to object size
Field Handling	pulsed-good; continuous-poor
Laboratory Data Handling	good excellent if reference marks in view, automatic computer analysis possible

Table 1 (Cont'd)

Item	Data
Technology	
Source	pulsed laser-1 joule, 30 nsec "Q" switch 10 joule, 1 msec normal
Location	pulsed-on prime mover or fixed to field (portable) continuous-fixed to field (portable)
Time for Field Setup	short most time spent in laboratory
Reference Marks	diffuse reflectors on field
Calibration	variable wedge placed in field
Maintenance	pulsed laser can damage optical components
Safety	only problem with high-energy pulsed laser sources which must be shielded operators can wear goggles for eye protection
Environmental Factors	condensation and dust on optics will require some cleaning or shielding vibration may be problem with any continuous laser holography arrangement air current and turbulence effects can be minimized if arrangement nearly normal to surface

Table 2

KEY PARAMETERS--LIVE-FRINGE HOLOGRAPHIC INTERFEROMETRY

Item	Data
Wavelength (λ)	continuous-633 nm; 515 nm; 488 nm
Sensitivity	$\lambda/8$ by interpolation to 1/4 fringe
Range	λ to 15λ where minimum is based on interpolation requirements and maximum is based on 30 fringes--motion of fringes also limits resolution more difficult
Repeatability	body motions error plus live fringe motion
Direction of Deformation	all least sensitive to motion out of place of reference and scene beams
Noise (speckle)	high speckle noise because small apertures are required to image fringes; speckle increases with reductions in aperture size
Noise (coherent)	low
Scene Distortion	several λ at edges is possible reduced by wet tank for holding plate
Fringe Visibility	poor low efficiency since laser is used for both reconstruction and illumination
Field Handling	poor pulsed systems for live fringe holography have not been developed for outside laboratory use
Laboratory Data Handling	complicated by large volume of data
Technology	
Source	continuous wave lasers only
Location	must be vibration isolated, fixed location only

Table 2 (Cont'd)

Item	Data
Time for Field Setup	photographic development is required on field
Replacement Reference	marker on object can be observed and illumination changed to eliminate extroveous fringes
Calibration	motion can be observed because of live fringe aspect
Environmental Factors	very sensitive to any air currents, temperature changes, vibrations, shocks, etc.

Table 3

KEY PARAMETERS--CONSTANT AMPLITUDE VIBRATION HOLOGRAPHIC INTERFEROMETRY

Item	Data
Wavelength (λ)	continuous wave lasers
Sensitivity	limited to $\lambda/2$ since interpolation is more difficult
Range	only λ to 5λ because intensity drops off rapidly and further fringes are difficult to detect
Repeatability	excellent
Direction of Deformation	normal to vibrating surface
Noise (speckle)	not a problem
Noise (coherent)	not a problem
Scene Distortion	moving object is not imaged but fringes are imaged scene is not necessarily observed
Fringe Visibility	good to poor and varies with order
Field Handling	must control vibration amplitude to applicable range so driver must be adjusted to get right value
Laboratory Data Handling	more difficult because of Bessel function dependence
Technology	
Source	continuous
Location	fixed to single location
Time for Field Setup	low
Replacement Reference	none used--a single exposure
Calibration	must use vibrating surface for calibration
Environmental Factors	usual for continuous wave holography except some vibration problems are relaxed

Table 4

KEY PARAMETERS--DUAL-FREQUENCY HOLOGRAPHIC CONTOURING

Item	Data
Wavelength	dual wavelength with 0.1 nm spacing near 694 nm for pulsed ruby laser and etalon control of modes; also 488 nm and 515 nm with argon-ion
Sensitivity	pulsed--1 mm to 1 cm
Range	same as other holography but use limited by depth of focus of camera
Repeatability	within one contour spacing possible but depends on replacement for moire
Direction of Deformation	normal to surface if moire used
Noise	similar to holographic interferometry
Scene Distortion	holographic
Fringe Visibility	pulsed source etalon control; may give some loss in visibility
Field Handling	good if pulsed source poor if continuous source
Laboratory Data Handling	moire used resolution determined by moire factors
Technology	
Source	ruby pulsed laser gives sensitivities which are variable but coarse
Location	pulsed could be on prime mover
Reference	markers on field
Calibration	place wedge on field between exposures
Safety	typical pulsed laser problems
Environmental Factors	must consider index variations on data

Table 5

KEY PARAMETERS--SHADOW GRID MOIRE CONTOURING

Item	Data
Wavelength (1/p)	p is pitch of grid
Sensitivity	1/p with interpolation to less possible
Range	limited by diffraction effects on shadow
Area	limited by grid size construction
Repeatability	good motion of grid during exposure reduces noise and has no effect on contours otherwise
Direction of Deformation	normal to grid plane only
Noise (speckle)	none
Noise (coherent)	none
Scene Distortion	limited by camera only
Fringe Visibility	fair but to achieve high visibility the grid should have same reflectivity as scene
Field Handling	simple motion of large grids may cause some distortion if frames are insufficiently strong
Laboratory Data Handling	normal typical moire
Technology	
Source	noncoherent or coherent
Reference	can leave frame in place
Calibration	addition of wedge to field of view
Environmental Factors	thermal expansion of frames humidity effect on grid material

Table 6

KEY PARAMETERS--INCOHERENT PROJECTED GRID

Item	Data
Sensitivity (1/p)	pitches of 1000 lines/mm to 1 line/mm Ronchi rulings are available
Range	limited by depth of focus of projector
Area	is limited by projector lenses
Direction of Deformation	normal to reference surface only
Noise (speckle)	none
Noise (coherent)	none
Fringe Visibility	varies with scene reflectivity
Field Handling	simple to apply; double exposure would require stable platform in field
Laboratory Data Handling	requires realignment of photographs by optics system
Technology	
Source	incoherent
Reference	markers on field
Calibration	wedge added to scene
Environmental Factors	little complexity in system so effects should be minimal

Table 7

COHERENT PROJECTED GRID

Item	Data
Sensitivity	about 1/p where the pitch is achieved by projection of two coherent beams at an angle to each other; can obtain ~ λ of source to centimeters for pitches
Range and Area	no depth of focus problems with coherent grid projection because light planes are projected to surface
Repeatability	must replace to within 1/p in same direction but motion allowed in other directions
Direction of Deformation	normal to surface only
Noise (speckle)	yes, but can be made small by proper photography of grid
Noise (coherent)	yes, but can be reduced by spatial filtering
Visibility	any moire technique has some visibility problems coherent grid projection has some added noise
Field Handling	much better than holography because of simplicity of method
Laboratory Data Handling	typical moire
Technology	
Source	pulsed or continuous lasers
Time for Field Setup	must make check of light plane pitch projection
Reference	marker on field
Calibration	wedge added to scene
Safety	typical pulsed laser safety limitations
Environmental Factors	effects of air currents are reduced as sensitivity is reduced

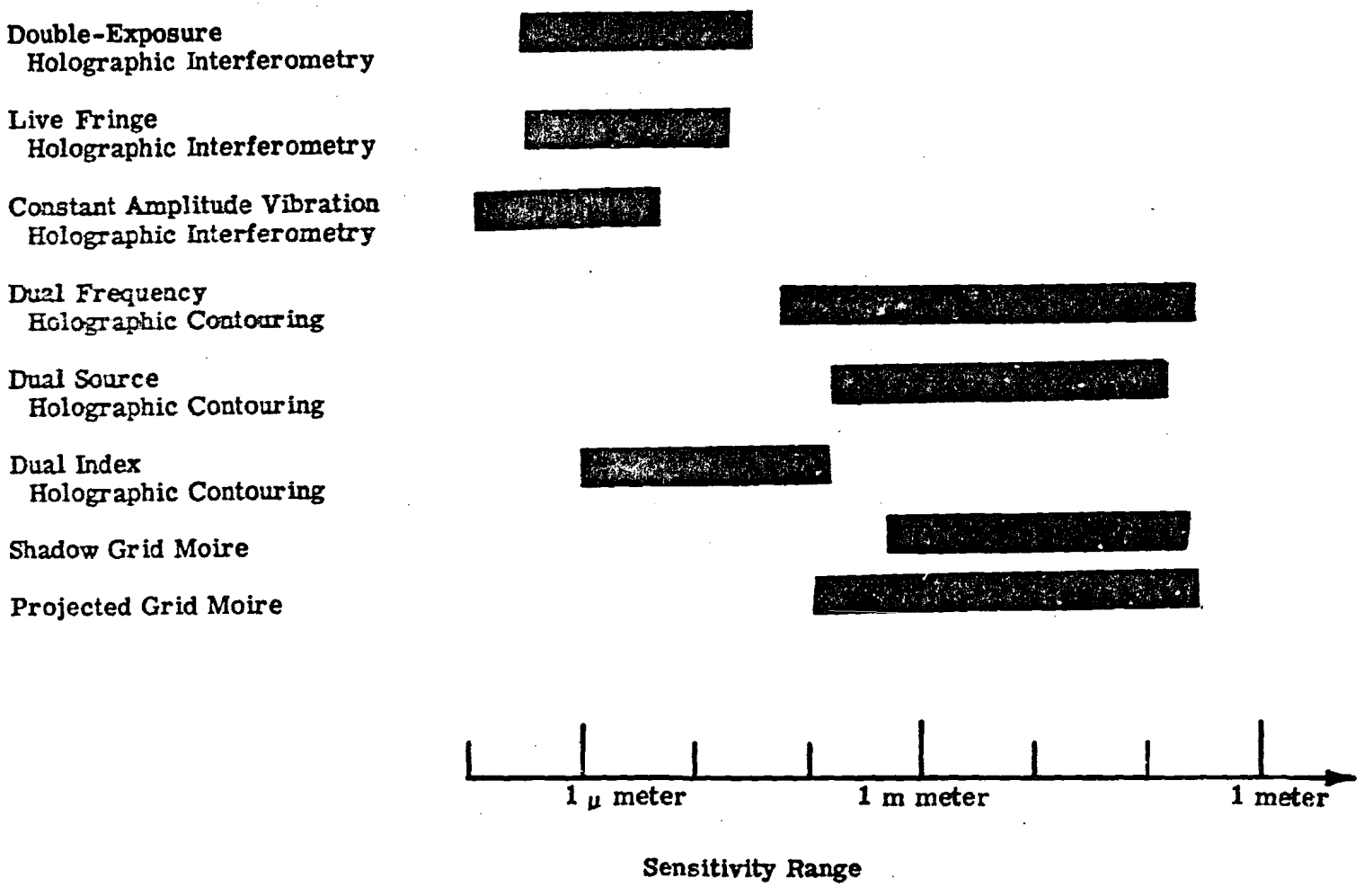

Figure 3 Resolution Range of Deformation Contouring Methods

SECTION IV

DEFORMATION CONTOUR GENERATION: EXPERIMENTAL RESULTS

1. General Experimental Consideration

There are several laboratory methods which demonstrate the technical problems involved with deformation contouring of runways. Here we describe experiments which use pulsed-laser and continuous-laser sources both for holographic and moire contouring methods. By doing this we hope to produce examples whose techniques include most of the complexities of the methods which are not demonstrated. The coherent-grid projection moire method demonstrates the moire methods, continuous laser use, and shows the results obtainable with dual-source holography. Dual-wavelength holographic contouring includes pulsed holography and ruby laser use. It also gives results similar to that of dual-index holographic contouring. Examples of the use of holographic interferometry methods are not given here because of the numerous examples previously published by the author of this report.

2. Projected-Grid Moire Experiment

The purpose of this experiment was to produce deformation contours of a runway model and to demonstrate the principles of moire testing. Also, a constraint was accepted in the work in that readily available equipment used in other projects was to be used and cost kept to a minimum. Therefore, this experiment does not represent the optimum one but is intended only as

a demonstration of deformation contouring. Since the eventual field versions of this technique would require a three-dimensional arrangement where source, object, and receiver are not a single laboratory table, the arrangement given in Figure 4 was used. The table holding the equipment was vibration isolated, but the runway model was placed on the floor and was not vibration isolated. This should magnify any low-frequency vibration sensitivity of the moire method since motion between the table and the floor is not fixed but allowed to undergo low frequency oscillations. The laser used was a 50-mW HeNe laser, with 633-nm wavelength, and approximately a Gaussian power profile output. The coherence length of the laser was not measured directly, but a minimum value was determined by making a hologram and obtaining a bright reconstruction over a coherence length of at least 5 cm, which represents a bright scene over a 10-cm difference in reference and scene beams. This degree of coherence was not necessary for the coherent-grid projector but a minimum value had to be established.

The laser output was steered by mirrors into the coherent grid projector which is detailed in Figure 5. The projector used consisted of a spatial filter, a beamsplitter, two mirrors, and an expanding lens. The spatial filter consists of a microscope objective and a pinhole which we adjusted to remove any light from the output which is not parallel to the input beam. By this method any coherent noise prior to the spatial filter

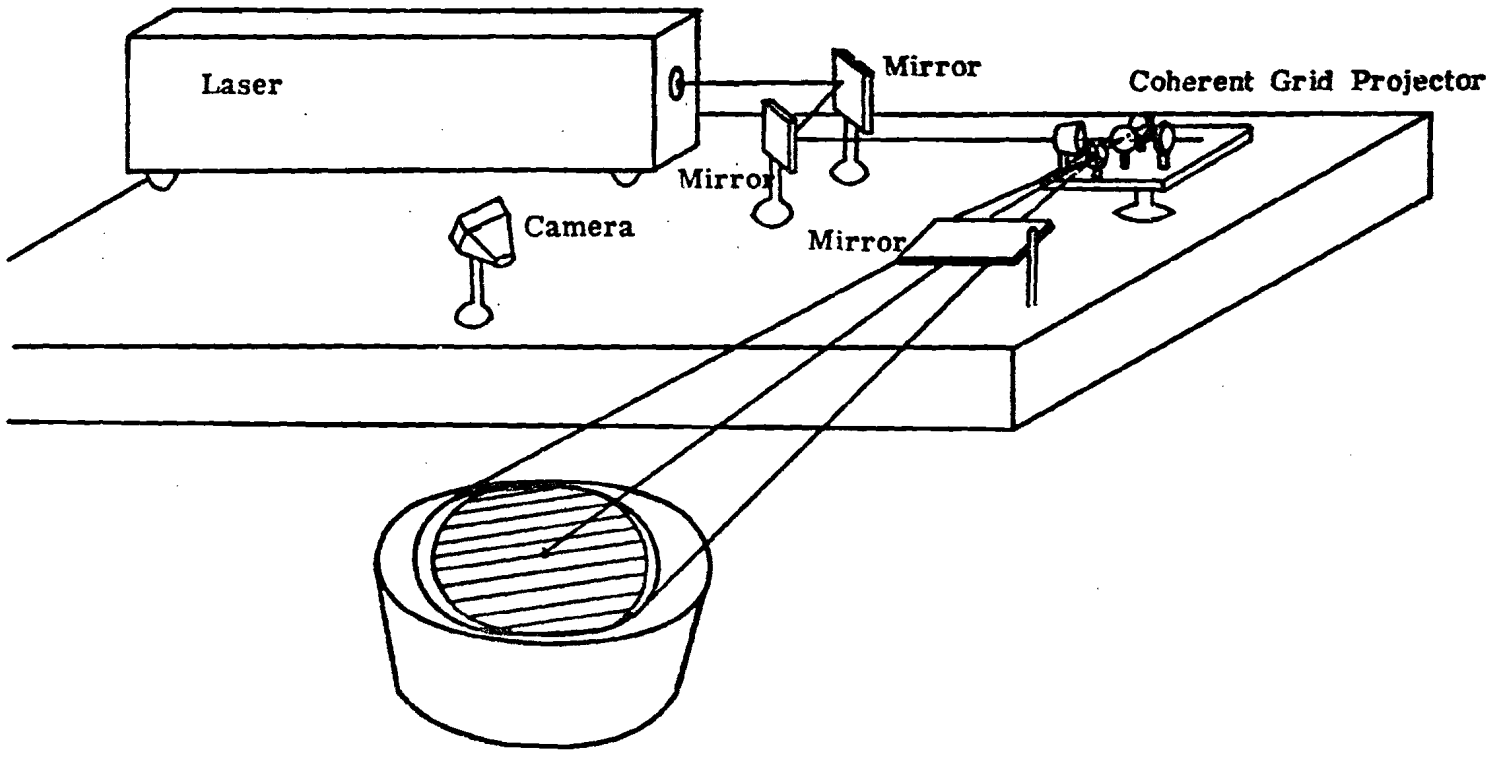

Figure 4. Moire Grid Deformation Contouring Arrangement.

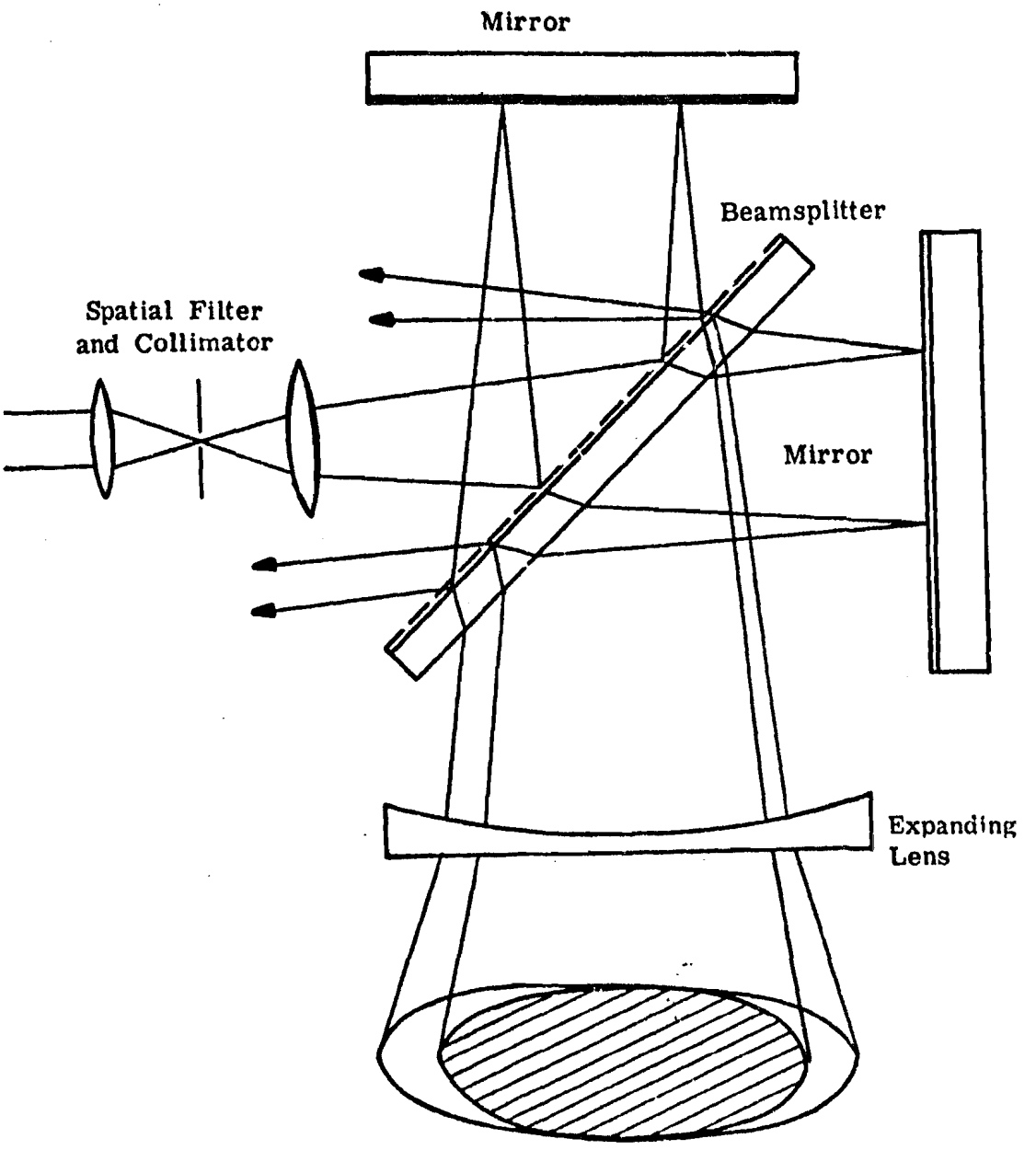

Figure 5. Detail of Coherent Grid Projector.

is removed and only coherent noise in the later stages can contribute. The low quality of this particular spatial filter prohibited the achievement of a noiseless input to the beamsplitter. The lens at the spatial filter output is used to collimate the beam back into a parallel beam. This lens also contributed to coherent noise because of multiple internal reflections. Additional coherent noise was introduced by multiple reflections in the beamsplitter. All these coherent noise additions can be removed by properly coating the optics for the wavelength used in the experiment.

The beamsplitter is a glass flat which is coated to reflect fifty percent and transmit fifty percent of the incident light. This transmission takes place twice since the mirrors return the beam through the beamsplitter. Note that one-half of the incident light is lost and exits in the opposite direction of the input beam. With proper adjustment this lost light could be used to provide a second exposure area and double the field. For this case only the normally exiting beams were used, and the projection of the two beams was made into the runway model by an expanding lens and a mirror. The mirrors are mounted so that screws can change the mirror angles with respect to the beamsplitter and with respect to each other. By varying these screws, the pitch and the orientation of the grid produced by their interference are changed. The desired pitch can be determined by a Ronchi grid held on the scene or by simple counting of the number of grid lines per centimeter.

Although the analysis equations from Appendix F were not used to determine an optimum camera position, it was observed that nil sensitivity was obtained if the grid was viewed from the locations near the grid projector where the cosine term $(\hat{s}\cdot\hat{v})$ is zero. The camera was located at a convenient location on the table and light planes adjusted to obtain good sensitivity to the deformations. The camera used was a simple view-finder camera with a ground glass screen for ease in observing the scene.

The runway model consisted of a tub of water covered with a vinyl sheet. This model gave localized deformations near loads whereas a simple membrane would have had deflections extending to the supporting edge and would not have simulated the localized deformation basin. Loads made of tantalum disks were placed in an assortment of loading patterns simulating aircraft wheel location. The membrane over fluid model was not intended to truly represent runways since no material parameters were considered. In fact, the almost undamped surface vibrations exhibited after load changes would not be considered to represent the runway physical situation.

The experimental procedure was to adjust the coherent grid projector and observe the grid on the ground glass of the camera and on the model surface. The pitch used during these experiments was 0.5/mm so the grid separation is 2 mm on the surface. By interpolation to one-tenth of a fringe the minimum resolution that could be hoped for is 0.2 mm (1/125 inch). This is not the best that can be achieved but matched the deformations produced

by the disk loads. When this pitch was obtained and the grid oriented for maximum sensitivity, the photographic film was exposed. After development it was replaced in the image position and the ground glass was removed. Moire fringes representing deformation contours could be observed by viewing the deformed grid through the filter produced by the first exposure. This process is explained in Appendix D and is the single-exposure case.

After the suitability of the arrangement was verified, double-exposure moire patterns were obtained by making a reference exposure, loading the model with a suitable arrangement of disks and making a second exposure on the film. Note that the surface vibration caused by loading the circular membrane over fluid continued during the second exposure and was of a low amplitude so that no adverse effects were made on the results. The continued vibration was detected by observing the speckle pattern variations which are far more sensitive than this particular arrangement for moire.

The double-exposure results are shown in Figures 6a through 6d where the double-exposure photographs are reproduced. The negatives produced had much higher visibility than the photographs produced from them, so the moire patterns are presented in a line drawing form to the right of the photographs to help the untrained eye in observation. The line drawing gives the lows of each dark and each light fringe.

Locus of Full- and Half-Order Fringes

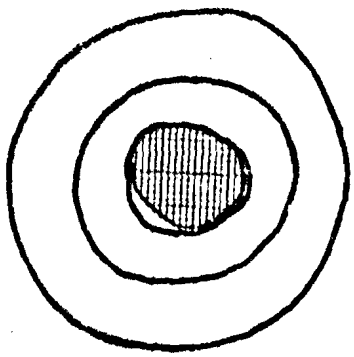

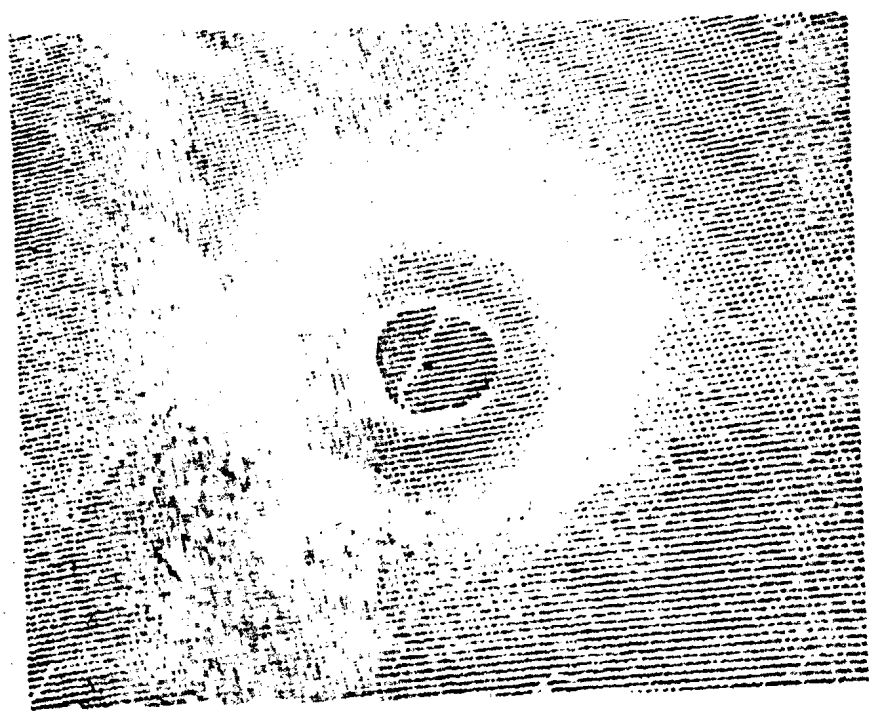

Original Moire

Figure 6a. Single-Disk Moire Deformation Contours.

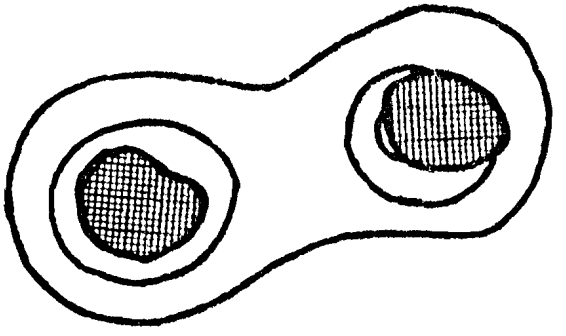

Locus of Full- and Half-Order Fringes

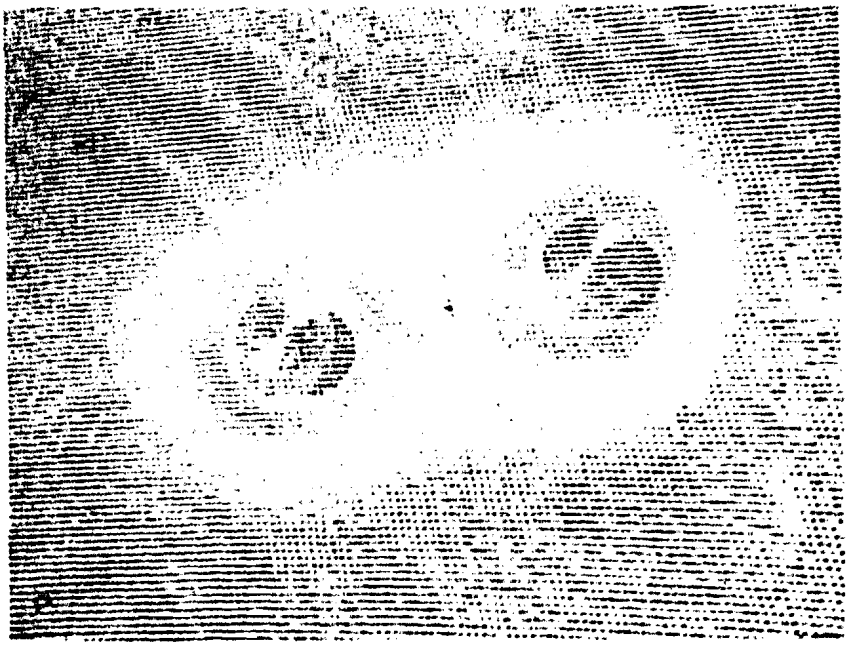

Original Moire

Figure 6b Double-Disk Moire Deformation Contours

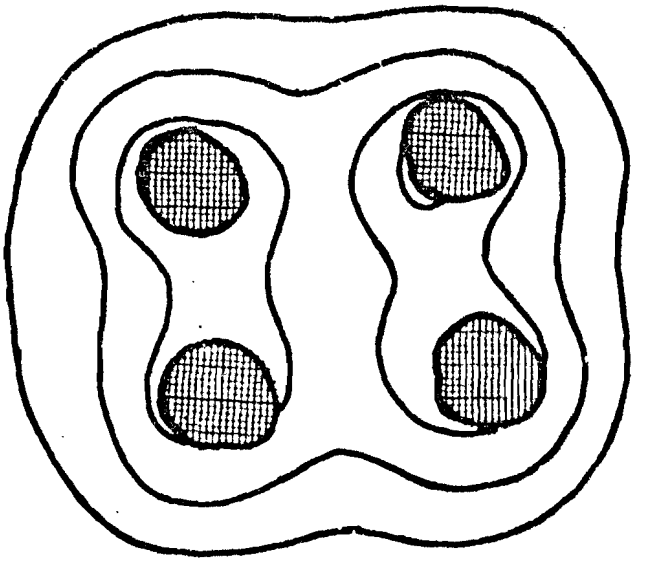

Locus of Full- and Half-Order Fringes

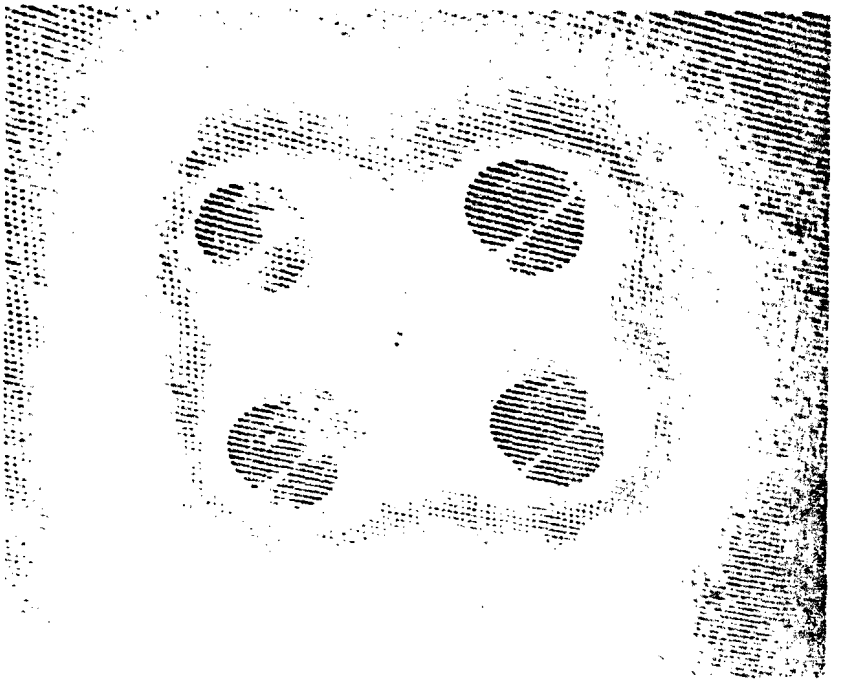

Original Moire

Figure 6c Four-Disk Moire Deformation Contours

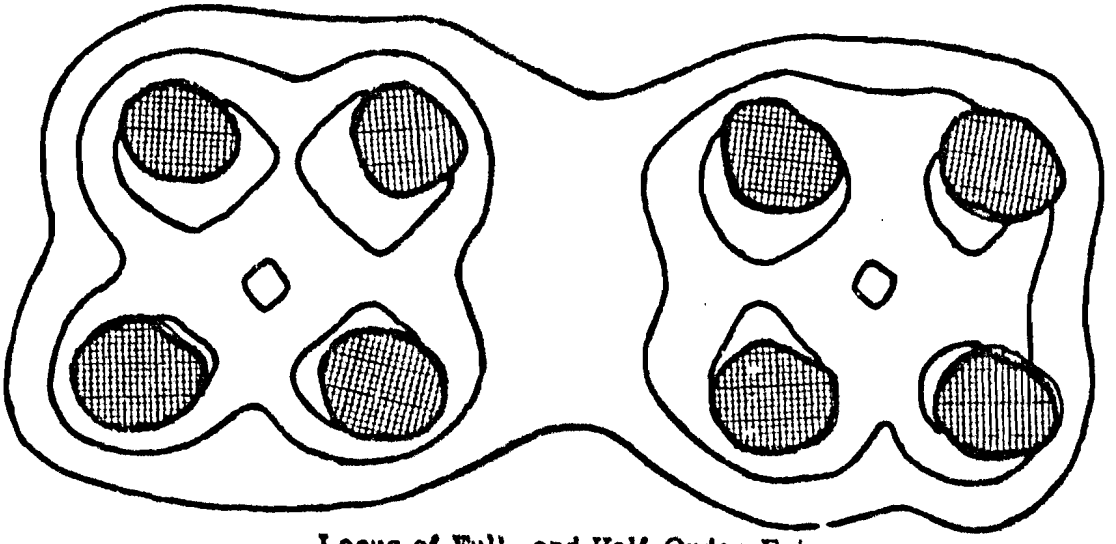

Locus of Full- and Half-Order Fringes

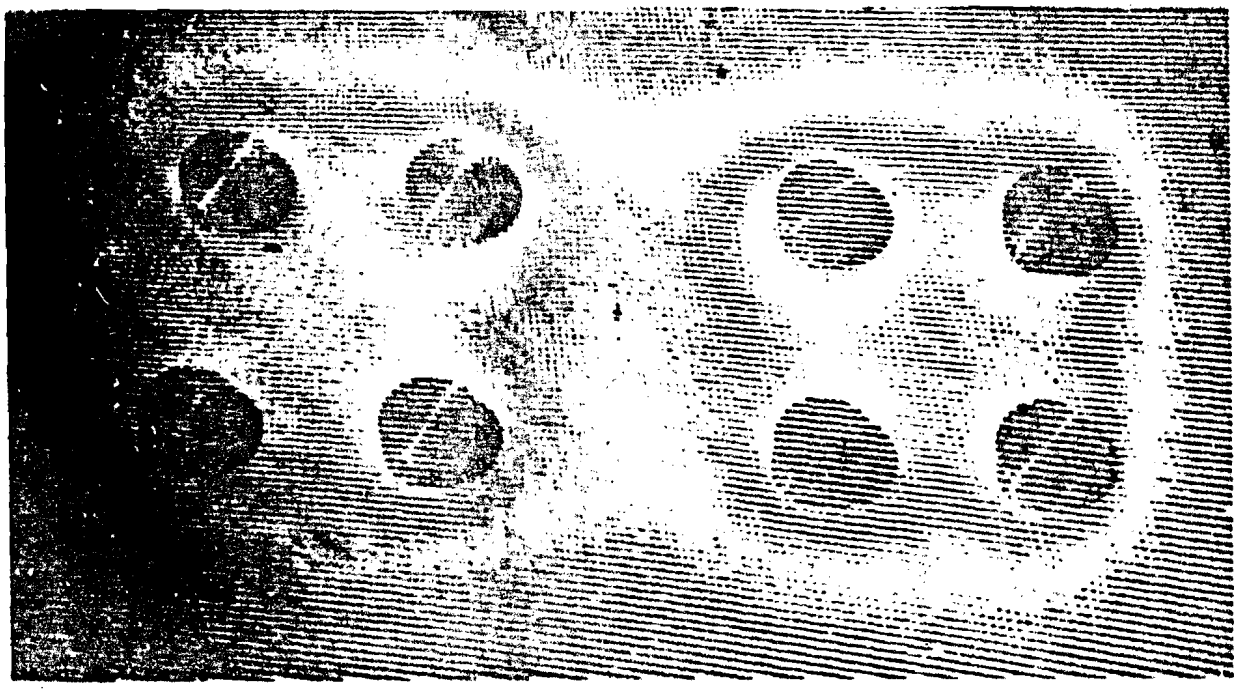

Original Moire

Figure 6d Eight-Disk Moire Deformation Contours

By recording the cartesian coordinates of the camera and the apparent location of the source behind the mirror, we can find the angles needed to analyze the moire contours. The coordinate system had its center in the center of the model surface. The results of analyzing the load patterns are given in Figures 7a through 7d where plots of deformation versus x positions are given for various positive y values.

The analysis of the fringes was made using a field fixed coordinate system instead of a load-based coordinate system in order to make a single calculation of analysis angles for all the loading patterns. This is evidenced in Figures 6b and 7b in the asymmetry of the two deflection minima along a given y coordinate. For this case the disks were not placed properly on the model surface and the center line of the loading pattern is not parallel to the y axis. Analysis with respect to a coordinate system defined by the center line of the two weights is not difficult if they are in view. The analysis for this case was performed by using the positions of the full- and half-order points with interpolation used only for finding minima or maxima values of deformation. Note the crosshatched region obscured by the weight and its shadow where no data can be taken. An alternative approach to analysis is the interpolation of orders for fixed positions.

The double-disk loading experiment was repeated with a similar geometry but with a stack of four disks at each load point.

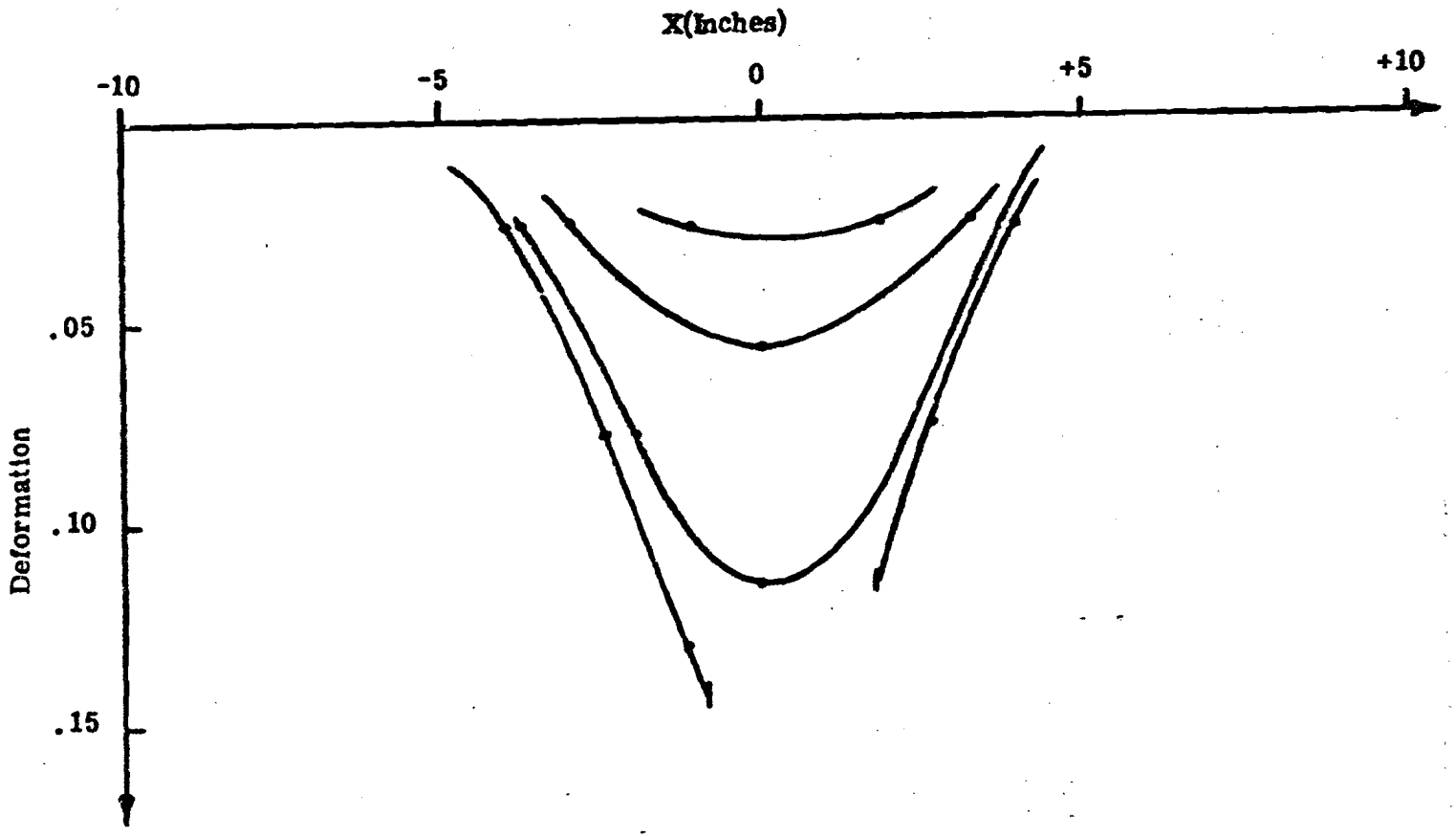

Figure 7a Deformation Due to Single-Disk Load

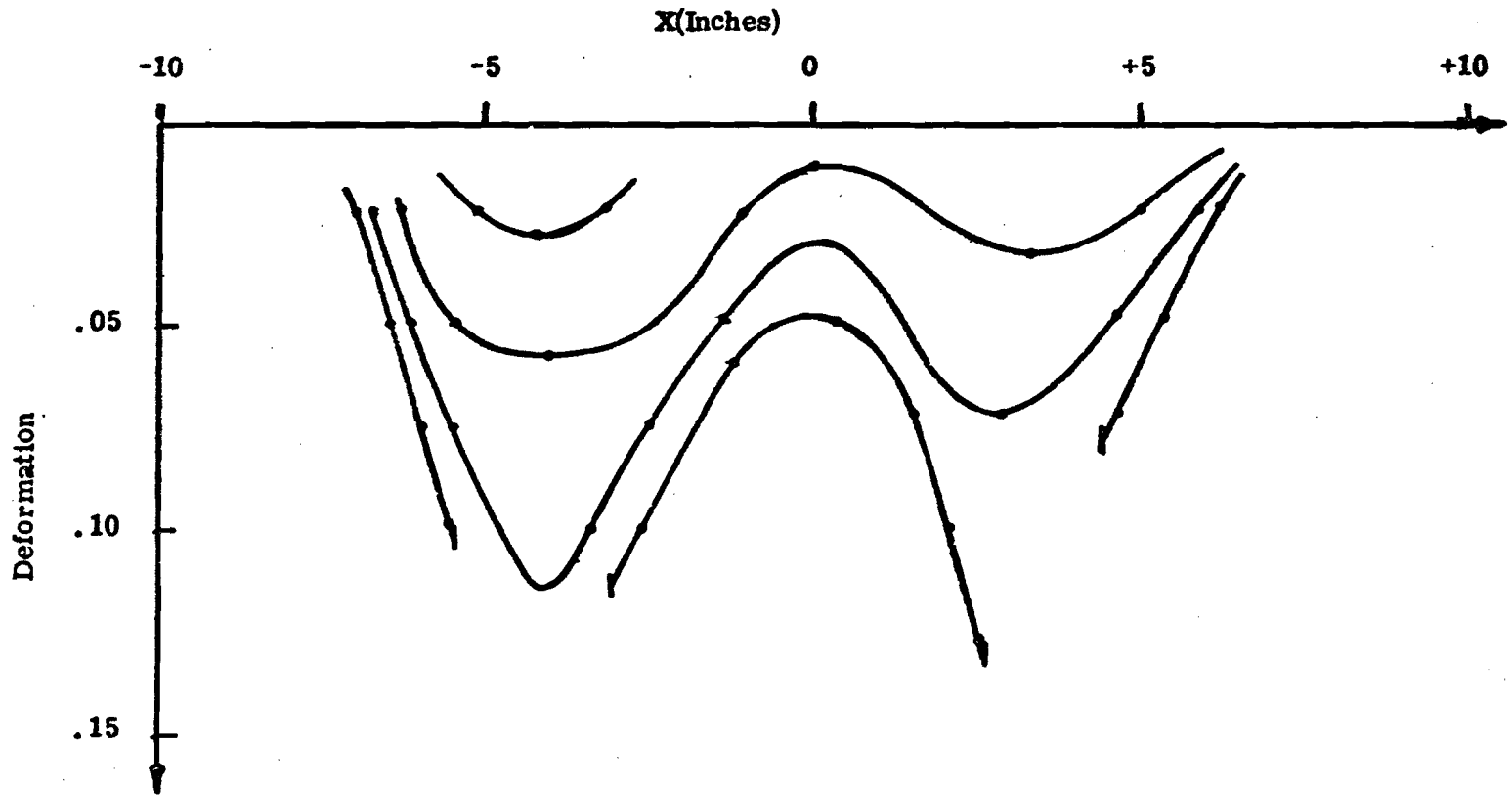

Figure 7b Deformation Due to Dual-Disk Load

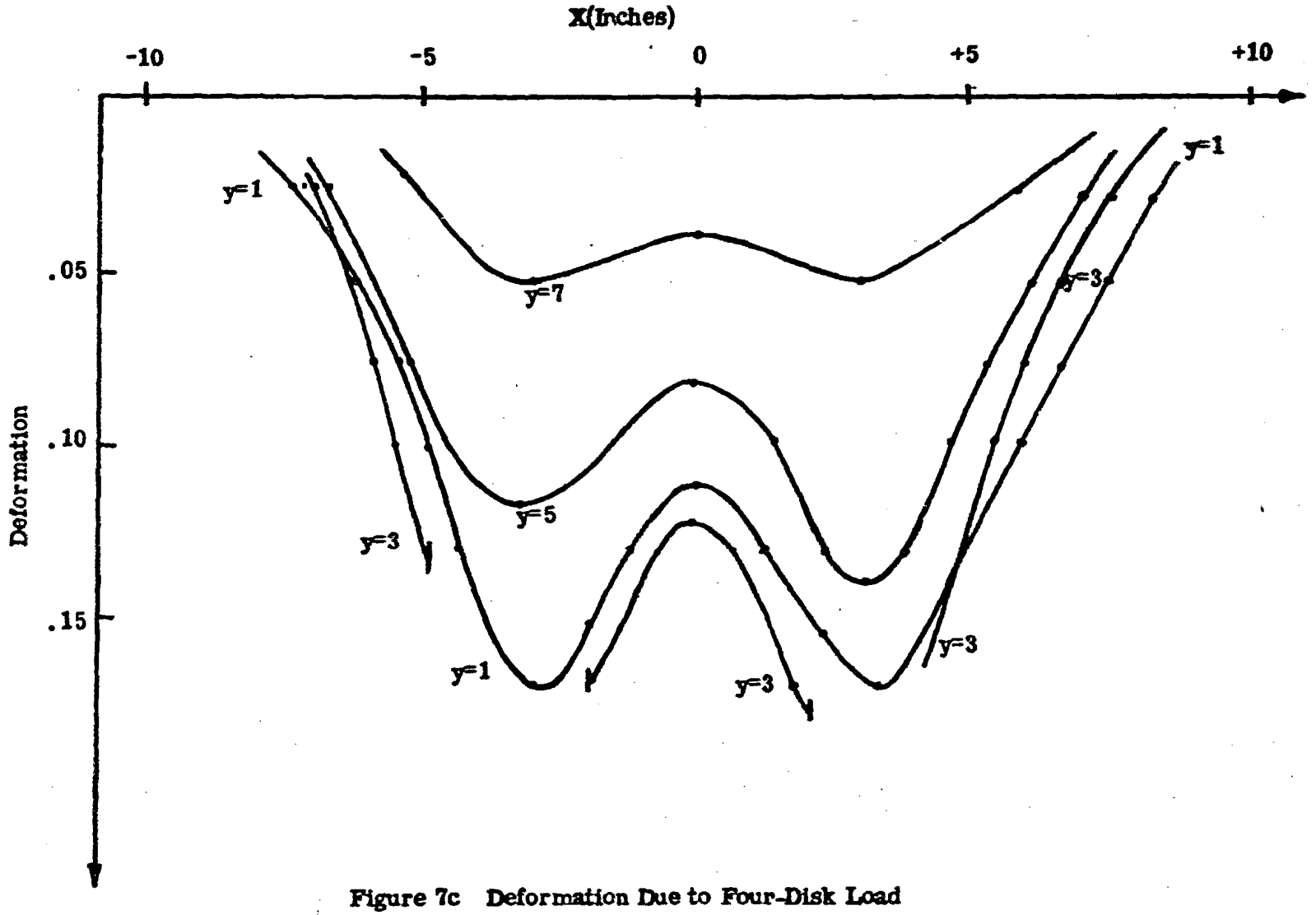

Figure 7c Deformation Due to Four-Disk Load

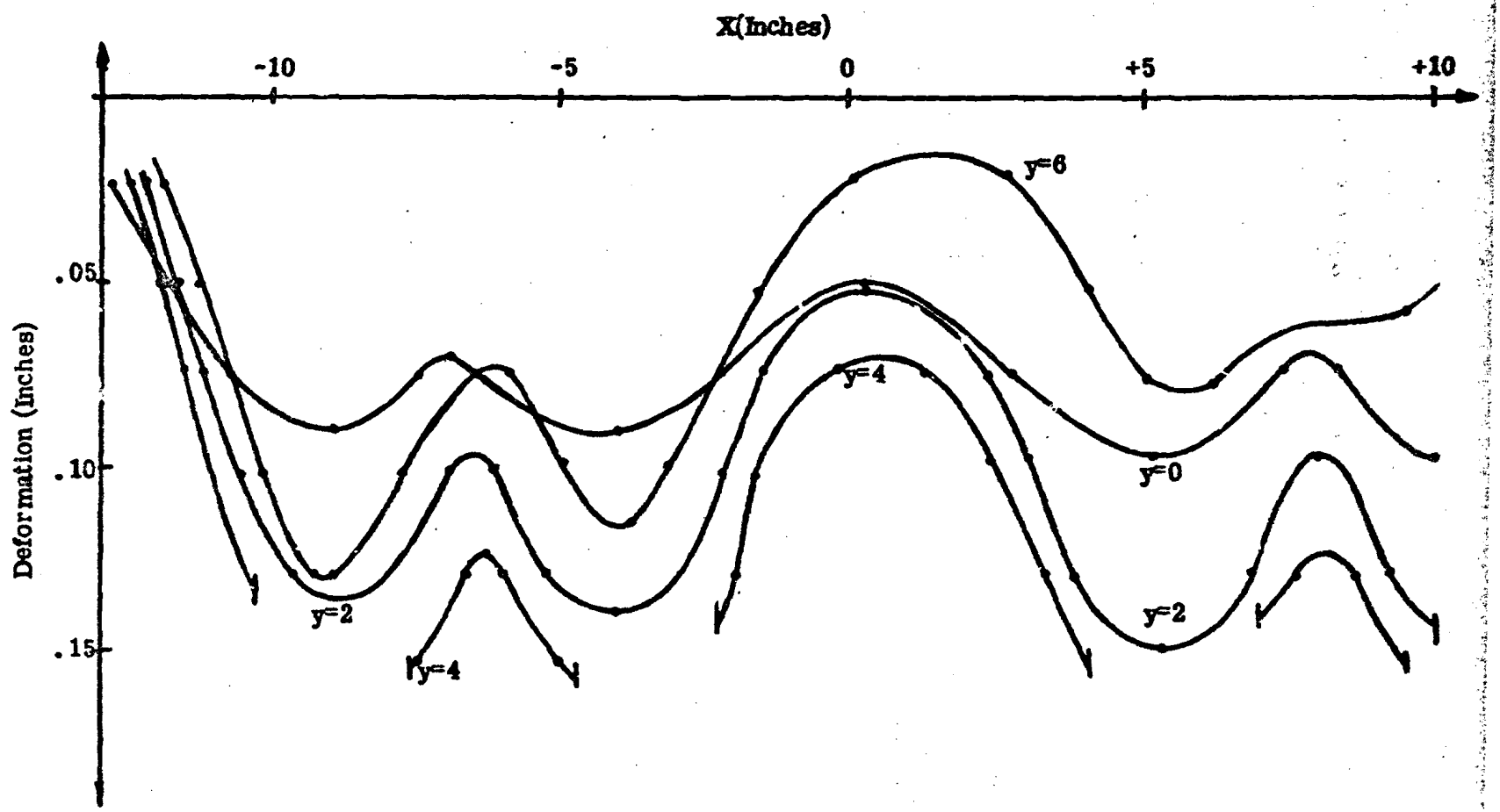

Figure 7d Deformation Due to Eight-Disk Load

The results of this experiment are given in Figures 8a and 8b. A comparison should be made with Figures 6b and Figure 7b where the deformation contours for the lower weights are given.

3. Dual-Wavelength Holographic Contouring Experiment

An arrangement for producing dual-frequency holographic contours of the model runway is given in Figure 9. It is similar to the previous arrangement except for the complexity added by the reference beam. Also, the pulsed laser components are included because they are manipulated to achieve dual frequency laser operation. Two common lab tables were used in an "L" shape and no vibration isolation was present. The pulsed ruby laser was "Q" switched by the Pockel's cell polarization rotator and stack polarizer. The ruby rod was not of holographic quality, but a series of tests were performed to locate a small portion of the ~ 1.25-cm diameter rod that would act with holographic quality and have acceptable phase uniformity in the output. This region was selected by a small aperture, about 2 mm in diameter, placed in the laser optical cavity. The helical coil flash lamp does help by ensuring a uniform rod pumping.

The optical cavity is formed by the 100 percent near reflector and the sapphire etalon at the output. The sapphire etalon is an optical flat made of sapphire and looks like ordinary glass to the eye. However, it is a crystal (ruby is sapphire with additional impurities to give a pink color and energy levels suitable

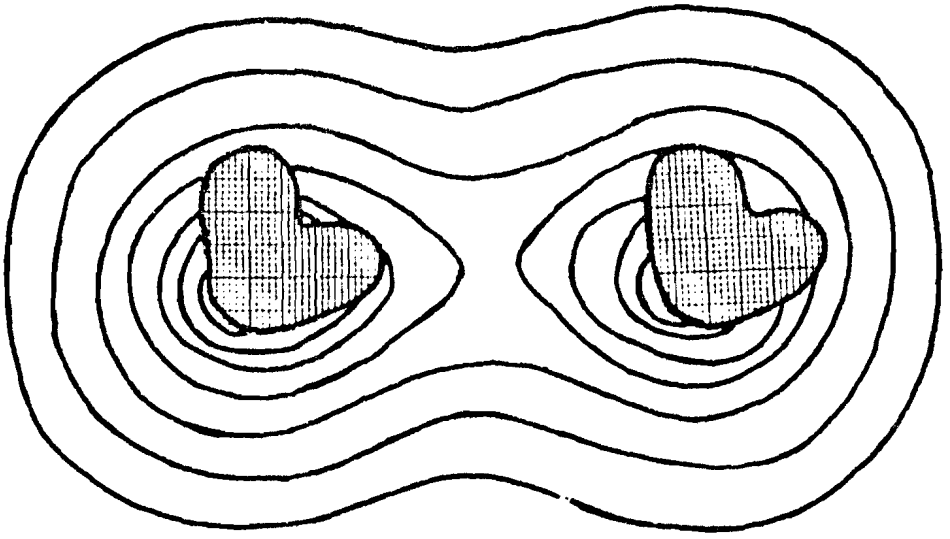

Locus of Full- and Half-Order Fringes

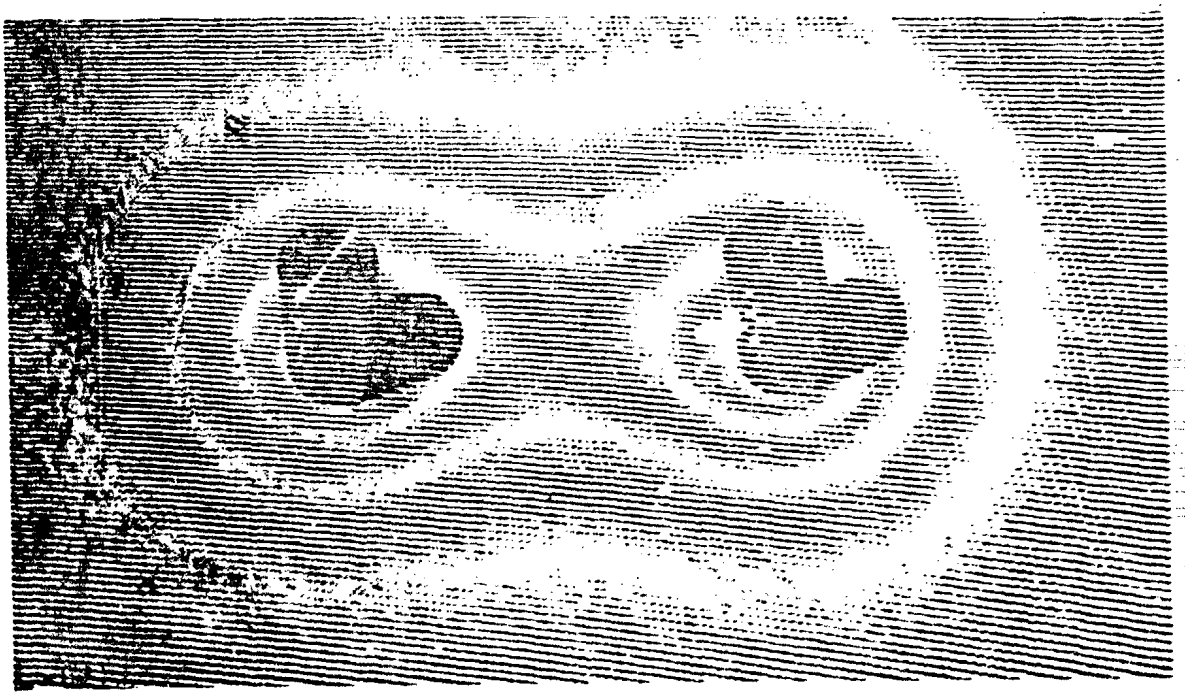

Original Moire

Figure 8a Double-Disk Moire Deformation Contours with Increased Load

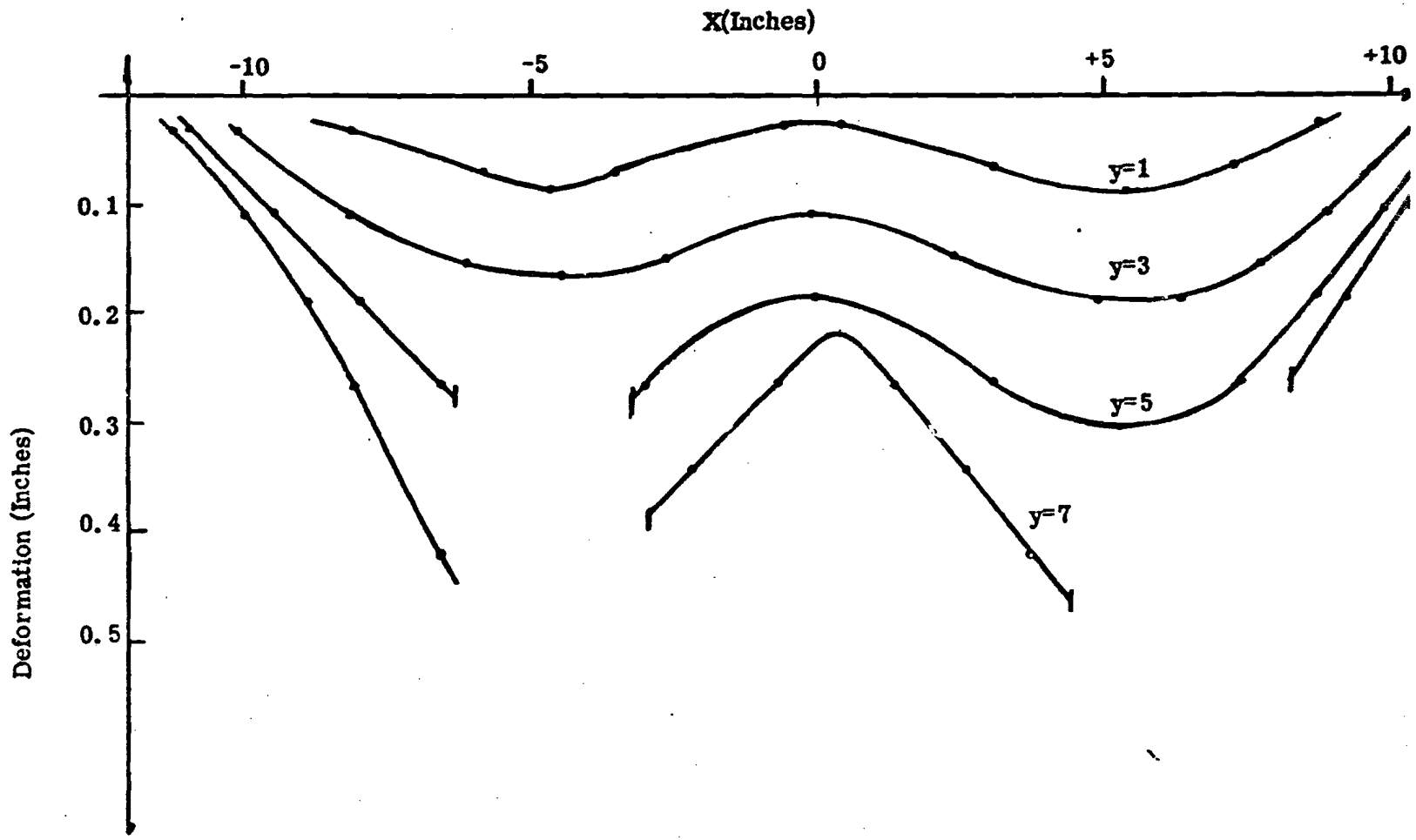

Figure 8b Increased Load Dual-Disk Deformation

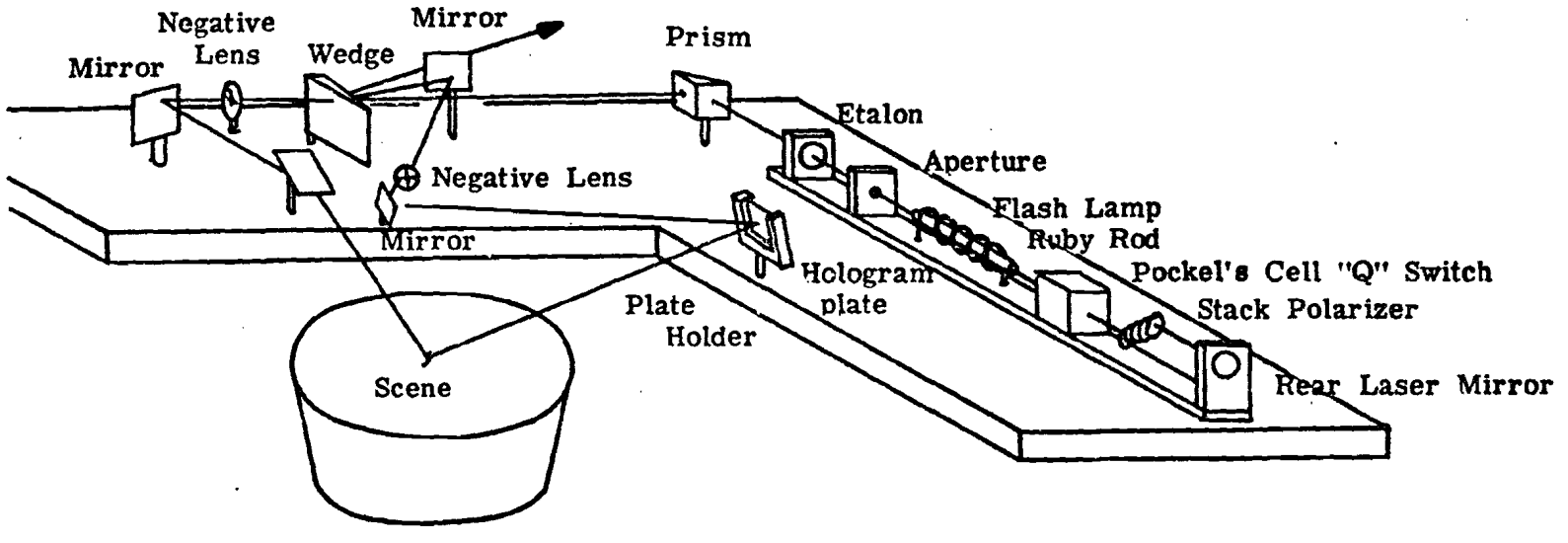

Figure 9. Dual-Wavelength Holographic Contouring Arrangement.

for lasing). The polarization axis must be adjusted properly to align with those of the ruby rod, and the glass is aligned with its faces parallel to those of the rod. The reflectivity of the sapphire is high because of its high index compared to ordinary types of optical glass and each of its two surfaces returns about eight percent of the light into the laser cavity. These two surfaces form an etalon whose spacing determines the output wavelengths of the laser. By correctly manipulating the etalon spacing and changing the flashlamp pumping energy, the laser may be made to operate with single or multiple wavelength outputs. A double etalon made of two sapphire etalons is commonly used to extend the coherence length of the laser by narrowing the width of the output wavelength. For this experiment single and double etalons were used and the spacing varied to obtain dual-wavelength contours. Also, a thermoelectric cooler was attached to a single etalon mount and a dual-frequency mode was selected by varying the etalon temperature.

A beam-turning prism is necessary for other high-energy applications of the laser but was used for convenience only for this application since only a small portion of the laser rod is used, and the resulting output energy is reduced to a small fraction of the possible output.

The wavelength selection gives an output which will contour the scene with spacing

$$\delta = \frac{\lambda_1 \lambda_2}{2|\lambda_2 - \lambda_1|}$$

from a reference position at the scene illumination source. The theory of etalons gives us an etalon optical spacing, s, requirement

$$ns = \frac{\lambda_1 \lambda_2}{2|\lambda_2 - \lambda_1|}$$

where n is the index of the etalon material. Therefore, the contour interval is related to the etalon spacing by

$$\delta = ns$$

The index of refraction of sapphire is 1.76, so with a sapphire etalon

$$\delta = 1.76s$$

where s is the thickness of the etalon. Since no sapphire etalons were available at less than about 2 mm, this experiment was limited in resolution to contour spacings of about 4 mm (apart from some geometrical factors).

A Herschel wedge was used as a beamsplitter. This wedge has a 10° angle and one high-quality optical surface. The

reflection from this surface is used as a reference beam source, and the reflection from the other surface is discarded. The reference beam was steered by mirrors and expanded by a lens with several criteria kept in mind: the reference path length must equal the scene path length, the angle between the reference and scene beams should be kept small, and the ratio of the reference to scene intensity should be kept between one and four. The first two criteria are met by changing mirror locations and the last by changing the expanding lens focal length. Without an evacuated region at the pinhole no spatial filter can be used in pulsed-laser applications.

The scene beam was manipulated to illuminate the model and reflect toward the holographic plate. The orientation of the holographic plate is such that its normal bisects the angle between the scene beam and the reference beam.

Figure 10 gives a typical photograph of the reconstructed contour produced by the pulsed ruby system. No attempts were made to produce moire deformation contours using this system because the sensitivity was not in the proper range to be applied to the deformations included in our model.

4. Evaluation of Experimental Results

The relative success of the projected-grid moire method as compared to dual wavelength holographic contouring in this laboratory feasibility study is due to the limitations of commercially available etalons. An additional limitation is

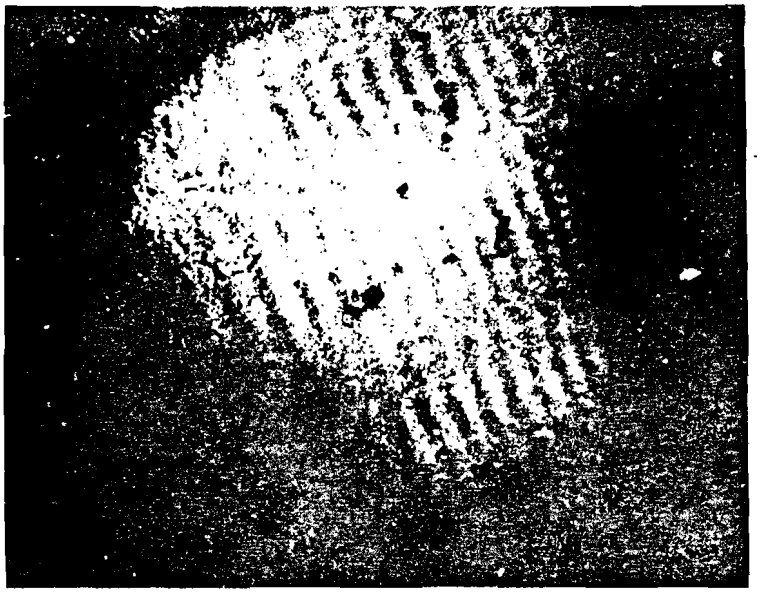

Figure 10. Contour Lines Produced by Ruby Laser Operating at Two Wavelengths

width of a single ruby fluorescent line. There are methods which can be further developed to operate the ruby laser in both of its ruby lines at once. These lines are centered at 694.3 nm and 693.1 nm giving a contour spacing of about 20μ meters. Therefore, a comparison of the relative success or failure of this experiment should not be of prime consideration in choosing one method over the other or for rejecting dual-wavelength holography for all applications of contouring.

SECTION V

CONCLUSIONS AND RECOMMENDATIONS

1. Choice of Alternative Methods

The experiment for dual-wavelength holographic contouring failed to establish a laboratory proof of applicability for deformation measurement, but the sensitivity limitations are well-known and methods of improving the sensitivity are not difficult. The scaling-up in size from model to runway can be made by the use of higher quality laser rods and laser amplifiers to provide the necessary energy. Also, the field application of holography by pulsed lasers has been made by the author. In sum, we feel that the application of holography to deformation contouring is possible. However, the moire method of deformation is technically easier to perform. The holographic considerations of high film resolution requirements and corresponding insensitivity are not necessary. The added complexity of providing a separate, high-quality reference beam is not required. The need for a long coherence length source is eliminated. The holographic methods are not as versatile since most laser sources have fixed wavelengths, and variation of contour spacings for changing deformation sensitivities is technically sophisticated. Continuously operating lasers can only be used with difficulty as sources for field operations because of the $\lambda/8$ vibration limitation. Therefore, we will assume that, except for special applications, the projected-grid moire method is to be applied to deformation

contouring of runways. The method has a minimum resolution and range of resolution matching runway deformation requirements and is not as difficult to implement as holographic interferometry.

2. Example System Engineering

We will show the feasibility of moire deformation contouring for runways and other field applications by a step-by-step consideration of critical factors.

The key factors in the field are the resolution, range, and area over which data can be collected. A prime consideration in the minimum resolution and maximum area is the laser speckle and camera depth-of-field relationship. The example used earlier gave 0.1-meter depth-of-field for a 0.1-mm grid spacing. Assuming interpolation between moire fringes thus represents a minimum resolution of about 10^{-2} mm (~ 0.4×10^{-3} inches). The area that can be included by a camera directly above the surface is limited by the 0.1 meter depth of focus. Assuming a height above the runway equal to the diameter of the area to be covered, we find the maximum difference in the distances to the camera

$$\Delta \ell = \sqrt{D^2 + (D/2)^2} - D$$

or approximately

$$\Delta \ell \simeq 1/8D$$

For the assumed geometry the depth of field is related to the difference in pathlengths by

$$\Delta D = \Delta \ell \sin(\tan^{-1} 1/2)$$

or

$$\Delta D \sim 1.125 \Delta \ell$$

Thus, the diameter of the area which can be photographed is about

$$D \sim 9 \Delta D$$

and for the example only a 0.9 meter diameter can be photographed with full visibility if laser speckle is not limited by some other means or the source resolution is sacrificed. This does not mean that data are not collected over additional area but that the effects of speckle can be observed if greater depth of field is used. For example, relaxation of the resolution requirement by a factor of 2.5 (minimum resolution at ab-ut 10^{-3} inches) yields a value of about 6 meters for diameter and camera distance, and this distance is for no significant effects of speckle and for full fringe visibility.

However, we assume the minimum resolution and suggest methods by which the speckle can be removed. The basic cause of laser speckle is the coherence of the laser beam. This coherence is necessary for producing the sharp interference from the dual source but introduces speckle noise if the coherence is high over the solid angle formed by the observer and a point of the object. One method of removing this coherence is to introduce a linear motion in the light source during exposure. Then the speckle averages out and does not deteriorate the fringe visibility. This can be achieved by moving the dual source parallel to the light planes during the exposure, thus averaging speckle out. Other methods are also feasible for reducing speckle if necessary to improve the moire fringe visibility in the region outside the minimal speckle diameter.

Coherent noise reduction can be achieved by proper care of optics and the use of spatial filters. If possible, the design of the coherent projector should be such that no components are placed in the optical path after the final spatial filtering. Any components placed after the final spatial filter must be kept clear of dust. Air motion may have to be induced over these elements to minimize coherent noise. Proper optical coatings are also required to eliminate undesired internal reflections in the elements and the resulting coherent noise and visibility losses when these additional sources are added to the desired dual sources.

We can find the effect of index changes along different paths by using the contour spacing

$$\delta = \frac{\lambda}{2\Delta n}$$

as was derived for use in dual-index holographic contouring. In order to apply it here the period of the grid, P, replaces λ. We will consider the effects of index variations by calculating the temperature gradient allowable across the scene. Vertical temperature and index gradients are larger but do not have significant effects on the results since they do not shift the fringes. We write

$$\Delta n = \frac{\partial n}{\partial T} \Delta T$$

where

$$\frac{\partial n}{\partial T} = \frac{3}{2} \left(\frac{n(n - 1)(n + 1)}{2n^2 + 1} \right) \beta$$

with

$$B = \frac{1}{v} \left(\frac{dv}{dT} \right)_p$$

(the isobaric thermal expansitivity). For gases $B \sim 10^{-3}\ {}^{o}K^{-1}$ and for air

$$(n - 1) = 3 \times 10^{-4}$$

giving

$$\frac{\partial n}{\partial T} = 3 \times 10^{-7}\ {}^{o}K^{-1}$$

and

$$\Delta n = 3 \times 10^{-7} \Delta T$$

The path over which one contour appears is then

$$\delta \cong \frac{\lambda}{2}\left(\frac{(3 \times 10^{6})}{\Delta T}\right)$$

For example, a $10^{o}K$ change in temperature would allow a 15-meter laser path before one interference fringe appeared in the data. We have assumed a relatively calm, night atmosphere. Further development would be required to determine the wind and thermal current conditions observed during daytime operation.

The problem of relocation of moire images is a further possible point of difficulty. For cases where locations on the ground are used and prime movers move through the test region, there is little difficulty in repositioning. The obvious solution is double-exposure moire but even better would be a dual camera which makes multiple exposures. Between exposures the dual source is shifted so that corrections to the final deformation contour map are minimal. Repositioning errors are also reduced by using the multiple-exposure method by using various optical processing techniques to shift one grid with respect to another. When location on the prime mover is required, the relocation of reference and deformed grids for moire is more difficult. The sensitivity to motion in the light planes is very small, but for minimum corrections to the deformation contours the repositioning must be withing a few grid periods. The exact accuracy of repositioning is determined by the deviation of the surface from a plane. In fact, for a flat there is no error in deformations due to repositioning errors in the plate; indeed, no first exposure is required and laboratory rulings may be used as references.

The system is calibrated by placing a wedge in the scene and making a moire deformation contour, with the wedge representing the deformation. Markings on the wedge would give depths and direct comparisons could be made with the deformation contour lines on the wedge. Several markers.

placed in the scene, would act as repositioning points. Other verification and comparisons of the moire deformation contours and contours from other methods should be made. In fact, a study of the effects of the holes bored for other types of deformation detectors should be included by making before- and after-deformation contour evaluations.

An additional key parameter is the total energy required from the coherent light source. This must be considered with respect to film sensitivity, exposure time to stop motion dynamic motions, background light, total deformation contour area, and safety. The film sensitivity is related to the film resolution. For a grid spacing on the field of 0.1 mm over a region of 2 meters diameter, the film must have a usable response of 200 lines/mm. This is not holographic quality but is higher than most ordinary films. A possible film is Kodak SO-243 with usable resolution to 500 lines/mm. About 0.3 erg/cm^2 are required to produce a density change of 1. Earlier we gave a relationship which we can use to solve for the laser energy required to expose the SO-243 film.

$$\varepsilon = \frac{E(r + 1)(a^2 + b^2)}{\rho}$$

where E is the required energy per unit area, a is the height above the field, b is the radius of the area to be photographed, ρ is the reflectivity, and r is a beam ratio used for holography

and is set to zero for this application. For a typical case of 2-meter diameter on the ground and a reflectivity of 0.25, we find

$$\varepsilon = 6 \times 10^{-3} \text{ joules}$$

Ignoring reciprocity failure, this can be achieved by any combination of continuous laser exposure and power or by pulsed lasers. The value of exposure time must be chosen to correspond to a stop motion of the grid so that only a small fraction of a grid spacing is allowed to change during the exposure. The noise due to background illumination is reduced by making shorter exposures. Since the energy requirement goes as the square of the area, a ten-meter radius on the ground would require a 0.6-joule exposure. These values may be halved for double exposure cases.

The operation of high-power pulsed lasers on the field requires a safety evaluation to ensure the protection of the eyesight of incidental persons. Operators should be required to wear laser safety goggles. A thorough checking of the area for specular reflectors and a screening of the specular reflection regions may be required to contain any possible specularly reflected laser beams.

Laboratory data handling would be facilitated by optical processing prior to providing raw data for the computer. Repositioning errors can be corrected by optical methods or by having

computer corrections to data. Also, contrast enhancement by optical or film processing can improve raw contour visibility. Schemes for changing the contour reference point by optical methods exist, but this transformation is easily handled by the computer. For small amounts of data only semi-automatic data analysis is necessary and an x-y position output device is the major equipment necessary for reasonable, speedy analysis. Automated picture digitizers are numerous (the author has built one such device) and would be required if a large number of data analyses are to be made.

3. Feasibility Conclusions

a. Feasibility

The usefulness of a scientific instrument is the major factor in determining its feasibility. The moire deformation contouring can yield, without any significant advances in the state-of-art, qualitative information of great utility. For example, detection of frost heaving locations, abnormal surface motion, detection of weakest points on the runway, etc., can be performed without concerning oneself with any advances in the state-of-art of moire optical techniques. Although these applications may justify the development of a moire device on their own accord, we must concern ourselves with the feasibility of producing a moire device for production of quantitative deformation contours with minimum grid spacing less than 0.1 mm

over an area larger than 3 meters in diameter and for operation under field environments.

There are three areas where further development and design data are required. First, the limitation on area of coverage due to laser speckle must be solved and the level of allowable speckle determined. Several approaches were suggested and require further efforts to determine the optimum solution to the speckle limitations. The effect of index variations of the air on the data was discussed here, but only field tests will determine the extremes of weather under which the loss of resolution is significant. Several possible solutions to the repositioning error correction were given. Again, it remains to be seen which method best solves the errors of inaccuracies in grid replacement. Finally, the operation of modern sophisticated optics, such as lasers and coated optics requires that special care be given in their selection, application, and maintenance.

We feel that due to the relative simplicity of the optics as compared to holography, past experiences in the application of holography in severe environments and the considerations given here that the quantitative application of moire deformation are feasible and that only present techniques need be selected for the optimum system.

b. Compatibility with Transfer Function Techniques

The data requirements for transfer function analysis of runways are such that whole field information is required to eliminate any errors due to shifting reference to the prime

mover. By using the whole field data from moire at positions with respect to the prime mover, the data are automatically in the prime-mover frame without any transformations. The examples used in this feasibility study have been aimed at a minimum resolution and an area corresponding to a typical width and depth of deformation basins, thus ensuring magnitude compatibility. Since data spacing can be chosen after the experiment, greater flexibility is achieved.

Indeed, there are studies underway which hope to produce vibratory prime movers. This new device may be even more compatible because only a single exposure is required to produce the deformation moire fringe patterns, and the problems of repositioning the reference grid are replaced by the simpler problems of longer exposures.

c. Suggestions for Further Development

Since there are several alternative approaches to improving the key factors in a moire deformation contouring device, we suggest a modular approach to further effort. First, a basic applicability module should be constructed. This device will be more limited in scope in that sacrifices are made in area coverage; however, the smaller sized and relatively inexpensive module can give design data upon which larger units for specific applications are constructed. Thus, after its use in determining optimum configurations for transfer function deformation contouring, it can be changed to provide both applicability tests and design data for other applications. By

investigating design alternatives with this module, the costs of the transfer function system are reduced and additional applications investigated without the dealys of waiting for gaps in usage of the transfer function system.

The flow chart in Figue 11 demonstrates the utility of the modular approach.

The basic applicability module should be a versatile system which can be adjusted to obtain the design information for a given case. For instance, a continuous wave laser of high power can be used in short exposure-small area applications or long exposure-large area ones. Since the unit is intended to provide design data, the use of different optical arrangements for dual source projection and photography is required. This unit would also be used to verify theory by checking derived analysis equations with known induced deformations.

The basic applicability module would consist of a system including the following items: The dual source, a camera receiver, an analysis system, optics for data enhancement, and a photographic processing laboratory. The dual source has several alternative designs so a building block optical system would be used to achieve versatility. Necessary equipment would be spatial filters, beamsplitters, optics, mirrors, and optical mounting hardware. Of course, a laser would be required for this system. The most obvious choice is an argon-ion laser due to the high powers obtainable from reasonably small sizes.

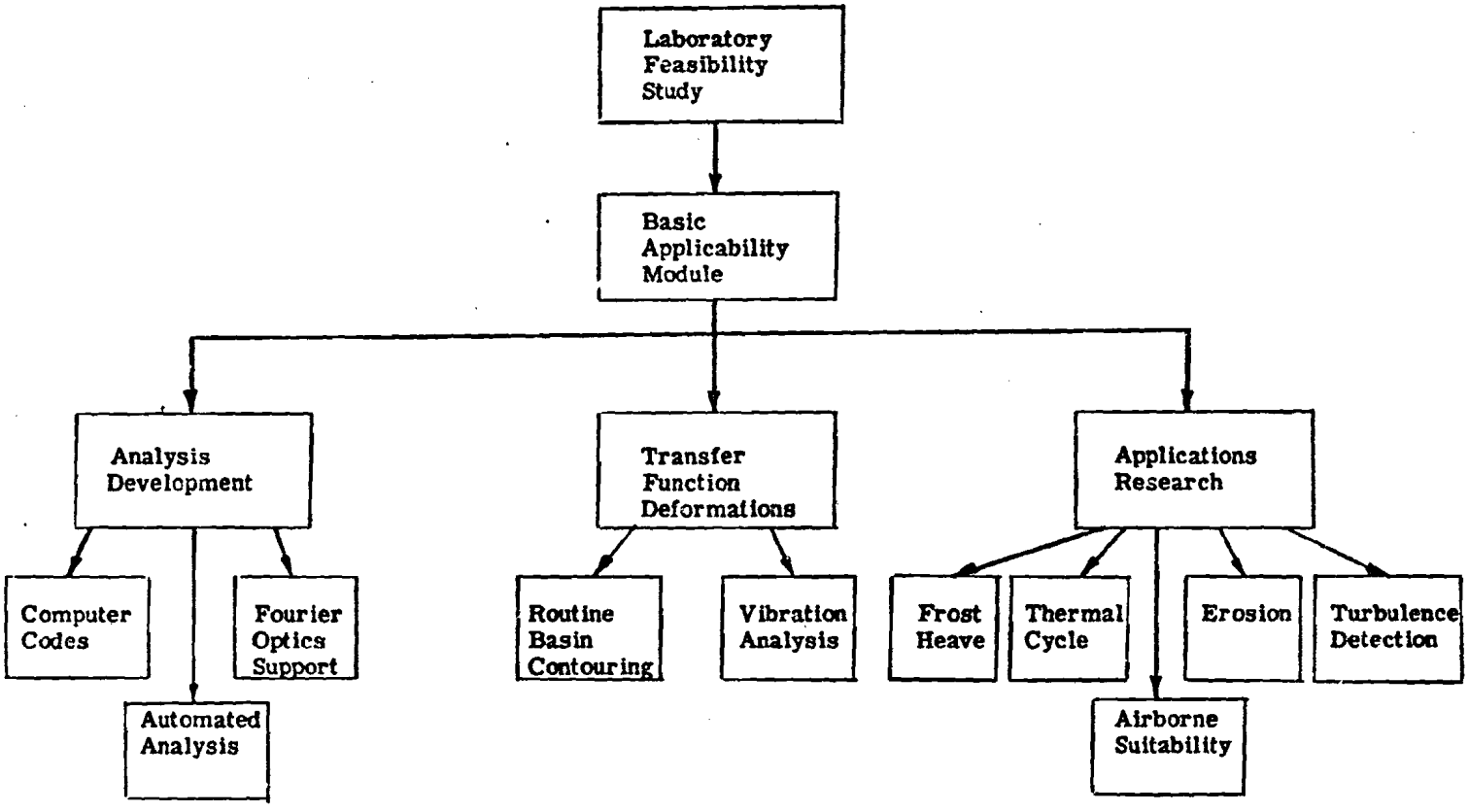

Figure 11. Development and Use Flow Chart.

The camera receiver must consist of two cameras because the filter method requires a camera to photograph the moire behind the reference camera. Also, the alternative approach of two cameras to eliminate replacement problems can be tried. Wedges and Ronchi rulings are required to perform calibration.

The analysis system should include analysis equations and a computer code. This code should be adaptable to allow for its application as a design aid. It can be used to find optimum source and receiver locations, to predict experiment results, and to solve for dual source locations required to give desired grid projections. A scheme should be developed for data collection so that automated data analysis is not required in these developmental stages. Also, an optical arrangement is needed to perform image enhancement, optical filtering and to test the methods of labroatory repositioning of the reference surface grid and the deformed surface grid.

After the design data are provided by the basic applicability module, the data would be used to build a system for contouring deformation basins. Since these basins are elliptical, several alternatives would exist and an advanced system would be made using a cost-effective approach. For instance, increases in the diameter of coverage may have significant break points in laser expense; and two smaller systems, each covering a little more than one-half the total area of the ellipse, may cost significantly less than one large system. The basic applicability module would allow for low risk in making evaluations like this.

The analysis of data from the basic research module would also provide a solid estimation as to the requirements of analysis computer code development, optical data enhancement, and automated data analysis systems.

APPENDIX A

HOLOGRAPHY

The basic principle of holography is that the wavefront from an object can be preserved by recording the interference between the wavefront and a reference beam. By reapplying the reference beam (called the reconstruction beam) the amplitude and phase of the original wavefront is reconstructed. In addition to the reconstructed wavefront, which for the case given here is perceived as a virtual image by the observer, a second wavefront, called the conjugate wavefront, is obtained. The conjugate wavefront gives a real pseudoscopic image of the object as shown in Figure 12. More complete discussion may be found in Smith or in Collier, et al. (see bibliography).

The intensity incident on the hologram plate of Figure 12 is due to two sources. The reference source, with complex amplitude $Re^{i\phi_r}$ and the amplitude scattered from the object $Oe^{i\phi_o}$. Since the light is coherent, the intensity is given by

$$I = \left(Re^{i\phi_r} + Oe^{i\phi_o}\right)\left(Re^{-i\phi_r} + Oe^{-i\phi_o}\right)$$

or

$$I = R^2 + O^2 + ROe^{(i\phi_r - i\phi_o)} + ROe^{-(i\phi_r - i\phi_o)}$$

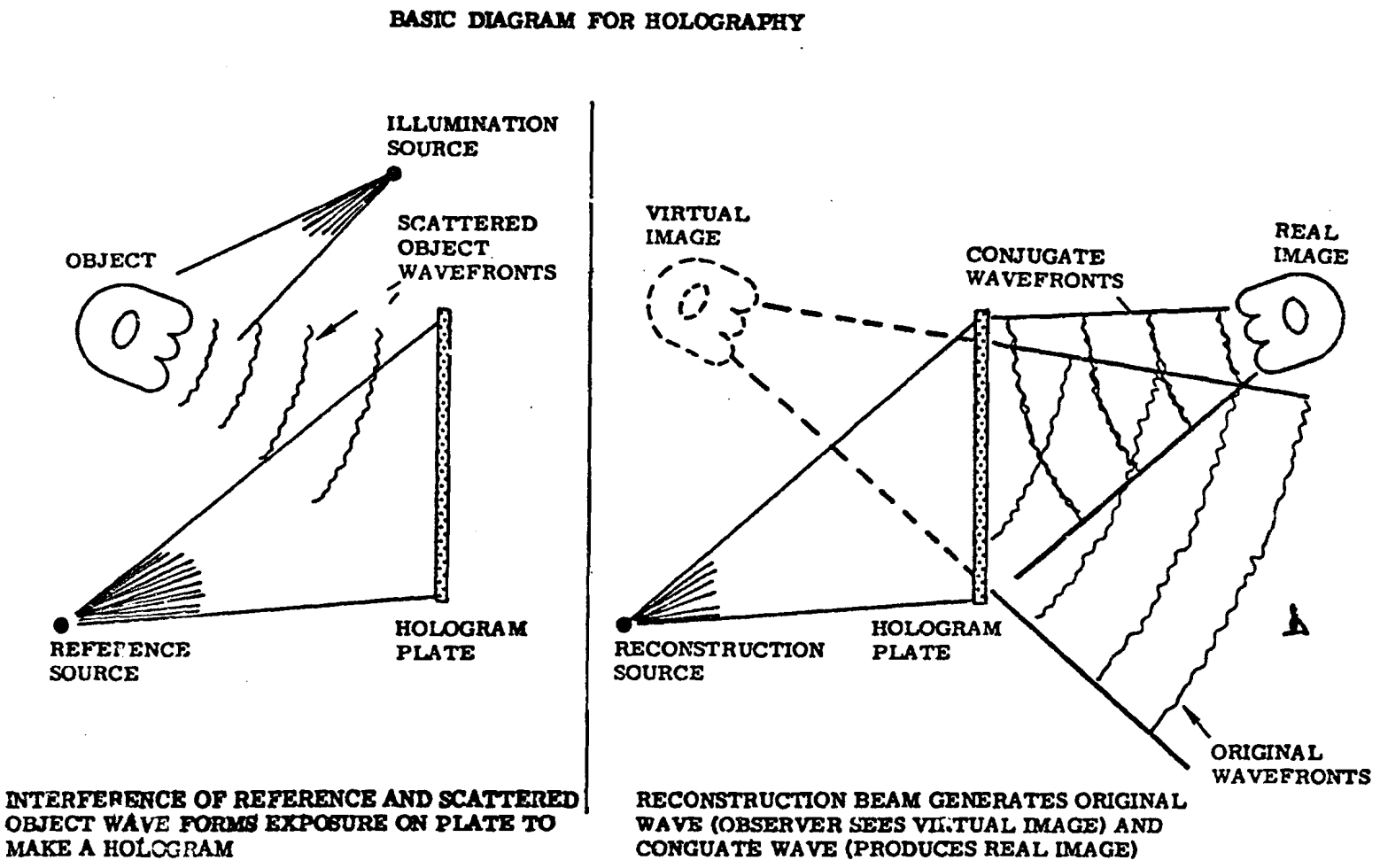

Figure 12. Basic Terms for Holography.

After developing, the amplitude transmittance of the hologram plate is given by

$$t = t_b + CROe^{i\phi_r - i\phi_o} + CROe^{-(i\phi_r - i\phi_o)}$$

where t_b is the result of terms without phase factors and C is a constant of proportionality. We now replace the plate and illuminate it with a wave identical to the original reference wave. The complex amplitude behind the plate is given by

$$A_p = t_b Re^{i\phi_r} + CR^2Oe^{i2\phi_r - i\phi_o} + CR^2Oe^{i\phi_o}$$

The final term in this amplitude is the original complex amplitude scattered from the object multiplied by a constant factor, CR^2. Thus, the original object wave has been reconstructed from the hologram plate. Note an assumption was made that the identical reference beam was used to reconstruct the object waves. Various error terms could be introduced if this is not true. Also, the photographic process is not a magic wand and the process described requires careful processing to achieve. However, in practice these problems are not usually serious and reasonable results are obtainable with a minimum of photographic care, as the extra terms introduced are not important in most applications.

The simple mathematics presented to describe the holographic process hides many subtle factors. The phase of reference and object waves vary with position on the plate and the angle of incidence of each is coded into the plate. Thus, the term t_b passes through the plate along the original reference beam direction, the term representing the reconstructed object wave is diffracted into its original direction, and the extra term is diffracted into some other direction depending on the phase terms. This extra term gives rise to a conjugate image since the phase of the object is reversed. If the object presents a virtual image, this conjugate wavefront usually gives a real image which can be intercepted with a screen.

APPENDIX B

HOLOGRAPHIC INTERFEROMETRY

The process of holography described in Appendix A can be used so that interferometric data is obtained. Double-exposure holographic interferometry is performed by making a hologram of an object which records the topology of the surface by the scattered wave. Then the object is deformed and a second exposure made on the holographic plate. Using the terminology given for holography for the process with subscript 1 for the first exposure and subscript 2 for the second, we obtain an amplitude transmittance

$$t = R_1^2 + O_1^2 + R_1 O_1 e^{i\phi_r - i\phi_1} + R_1 O_1 e^{-(i\phi_r - i\phi_1)}$$

$$+ R_2^2 + O_2^2 + R_2 O_2 e^{i\phi_r - i\phi_2} + R_2 O_2 e^{-(i\phi_r - i\phi_2)}$$

Assuming that the deformation has insignificant effect on the surface microstructure, we find that $O_1 \approx O_2$. The reference beam was identical in the two cases, so $R_1 = R_2$. Combining these gives

$$t = 2R^2 + 2O^2 + ROe^{i\phi_r - i\phi_1} + e^{i\phi_r - i\phi_2}$$

$$+ e^{-(i\phi_r - i\phi_1)} + e^{-(i\phi_r - i\phi_2)}$$

Applying the reconstruction wave gives an amplitude behind the plate

$$A_p = 2R^2Re^{i\phi_r} + 2O^2Re^{i\phi_r} + R^2O\left(e^{+i\phi_1} + e^{+i\phi_2}\right)$$
$$+ e^{+(i2\phi_r-\phi_1)} + e^{+(i2\phi_r-\phi_2)}$$

The terms of interest are the ones in the direction of the original object wave

$$O\left(e^{+i\phi_1} + e^{+i\phi_2}\right)$$

This represents a wave moving in the right direction with intensity

$$A_O = O^2\left(2 + e^{+i(\phi_1-\phi_2)} + e^{-i(\phi_1-\phi_2)}\right)$$

Using $\Delta\phi = \phi_1 - \phi_2$, we obtain

$$A_O = O^2(2 + 2\cos\Delta\phi)$$

Since the phase change $\Delta\phi$ is related to the optical path difference introduced by the deformation, it is a sensitive indicator of the deformation.

Live-fringe holographic interferometry yields similar data but is performed by making a single hologram and reconstructing the virtual image as a standard for comparison with the object as it is deformed. The object is illuminated and the reconstruction beam applied at the same time. The reconstructed standard object wave then interferes with the deformed object beam depending on optical path changes. Again we show the transmittance of the plate with our established terminology

$$t = R^2O^2 + ROe^{i\phi_r - i\phi_1} + ROe^{-(i\phi_r - i\phi_1)}$$

When reconstructed, we obtain

$$A_1 = R^3e^{i\phi_r} + RO^2e^{i\phi_r} + R^2Oe^{i2\phi_r - i\phi_1} + R^2Oe^{i\phi_1}$$

Adding the illumination to the object gives an additional term behind the plate due to the reilluminated deformed object

$$A_2 = R^2Oe^{i\phi_2} + O^3e^{i\phi_2} + RO^2e^{i\phi_r - i\phi_1 + i\phi_2}$$

$$+ RO^2e^{-(i\phi_r - i\phi_1 - i\phi_2)}$$

The intensity behind the plate is $I = (A_1 + A_2)(A_1 + A_2)^*$. Solving for the intensity in the object wave direction, we obtain

$$I_0 = 4(R^2O^2)(R^2 + O^2) \cos \Delta\phi + \text{constant}$$

or the result obtained for double exposure except for proportional factors and the addition of numerous terms in directions other than the object direction. Thus, both live-fringe and double-exposure holography techniques give a sensitive measure of light path changes with surface topology changes. For example, consider the deformation normal to a plane with angles of incidence θ_i from the illumination source and θ_s to the observer.

For a deformation Λ at a general position on the plane, we get an optical path difference

$$s = \Lambda(\sin \theta_i + \sin \theta_s)$$

The phase difference can be related to the path difference by

$$\phi = \frac{s}{\lambda} 2\pi$$

Solving for D and eliminating s gives

$$\Lambda = \frac{\phi}{2\pi(\sin \theta_i + \sin \theta_s)}$$

For small angles of incidence, the first dark fringe occurs at approximately $\lambda/4$, the second at $3\lambda/4$, etc. The deformation required to go from one dark to the next is $\lambda/2$ since the optical path changes at twice the rate of deformation. Since interpolation to 1/10 fringe is possible with a reasonably good accuracy, the method has precision of about $\lambda/20$, which is approximately 30 nanometers. The minimum detectable deformation is about $\lambda/4$ since the magnitude of the cosine term is unknown and must be established. The range is limited by the number of fringes observable and, therefore, depends on the geometry and spatial extent of the deformation.

Constant amplitude vibration can also be detected by holographic interferometry. Suppose we make holograms over a period of time much greater than the period of the vibrations of the object. We obtain the intensity at the plate.

$$I \propto R^2 + O(t)^2 + RO(t)e^{i\phi_r + i\phi(\tau)} + RO(t)e^{-(i\phi_r + i\phi(\tau))}$$

which must be averaged to obtain the exposure

$$\langle I \rangle = \frac{1}{P} \int_0^P I(\tau)\, dt$$

Reconstruction with the original reference beam and picking out the term with the object wave direction gives an amplitude behind the plate

$$A \propto \frac{1}{P} \int_{o}^{P} O(t) e^{i\phi_o(\tau)} \, d\tau$$

For small vibrations O(t) is a constant with time. For this case we write the phase shift to show the solution

$$\phi_o(\tau) = -\frac{2\pi}{\lambda} \Lambda (\cos \omega\tau) \left[\sin \theta_i + \sin \theta_s \right]$$

where λ is the wavelength, Λ is the displacement, θ_i and θ_s are the angles of incidence to the illuminating source and the observer and ω is the frequency of vibration. Substituting this and averaging, we obtain

$$A = \frac{2\pi}{\lambda} \int^{2\pi} e^{-\left(i\frac{2\pi}{\lambda}\Lambda(\sin\theta_i + \sin\theta_s)\cos\omega t\right)} d(\omega\tau)$$

or performing the integration we find

$$A \propto J_o \left[\frac{2\pi}{\lambda} \Lambda (\sin \theta_1 + \sin \theta_s) \right]$$

where J_o is the zero order Bessel function. The intensity observed goes as the square of the first order Bessel function, so the modulation of the image is not of uniform intensity but drop off fast as higher orders occur for larger deformations.

Live fringe constant amplitude vibration detection is also possible. This method is even more sensitive than the double exposure method since the first zero of the Bessel function occurs when the argument is approximately 2.4. Therefore, with $(\sin \theta_1 + \sin \theta_s) \sim 2$

$$\frac{4\pi}{\lambda} \Lambda = 2.4$$

at the first zero yielding

$$D \sim \frac{\lambda}{5}$$

Further, fringes must be evaluated using the zeros of the Bessel function instead of zeros of the cosine function as previously done. The total number of fringes which can be obtained is limited by the rapid decrease in intensity of $J_o(x)^2$ as x increases, and six or seven fringes are the most which have been experimentally observed unless nonlinear photography is used to bring out larger numbers.

APPENDIX C

MOIRE FRINGES

The modulation introduced by the superposition of two gratings is called a moire fringe. Here we will develop an expression for that modulation using the intensity that is transmitted by a sine wave grating with a plane wave incident upon it.

$$I(x) = \frac{1}{2} + \frac{1}{2}\sin(2\pi xp)$$

where x is the position perpendicular to the grating lines and p is the pitch (spatial frequency) of the grating p.

$$p = \frac{1}{L}$$

relates the pitch and distance between lines L. We have assumed geometrical optics for this relationship and its use when coherent illumination is used or very large pitches are present is risky. Diffraction effects are minimized because the grating is a sine wave and edges are soft. If two gratings with the same pitch are held together, the intensity behind the plate is the product of the two transmittances

$$I(x) = \left[\frac{1}{2} + \frac{1}{2}\sin(2\pi xp)\right]\cdot\left[\frac{1}{2} + \frac{1}{2}\sin\left(2\pi p(x + x_o)\right)\right]$$

where the phase shift representing the possible difference in origin, x, is given by $2\pi p x_o$. For the case where $x_o = 0, \frac{1}{p}, \frac{2}{p}$ we obtain the original intensity squared and would call this no fringe. For the case $x_o = \frac{1}{2p}, \frac{3}{2p}, \ldots$ we get

$$I(x) = \frac{1}{8}(1 - \cos 2x)$$

which is a double frequency-reduced amplitude signal over the entire scene and is called one dark fringe. If square wave gratings were used, the extinction would be total instead of the higher frequency reduced amplitude. For this case the full screen has the same fringe order.

An additional, more practical case is to have two different pitches in two gratings. The intensity directly behind the gratings is

$$I(x) = \left[\frac{1}{2} + \frac{1}{2}\sin(2\pi x p)\right] \cdot \left[\frac{1}{2} + \frac{1}{2}\sin\left(2\pi x(p + \Delta p)\right)\right]$$

For simplicity we have placed the origin so that any initial phase shift from offset is nulled, where Δp is the difference between the pitches of the two gratings. In this case the phase varies across the scene as $2\pi\Delta p x$, giving the transmitted intensity

$$I(x) = \frac{1}{\zeta}(1 + \sin 2\pi\Delta px)[1 + \sin(2\pi px)\cos(2\pi\Delta px)$$

$$- \cos(2\pi px)\sin(2\pi\Delta px)]$$

Now as x increases, the intensity changes from the no fringe to dark fringe condition and back. An example, produced by a line grating, is shown in Figure 13.

A third case is obtained when the gratings are rotated with respect to each other. Now we must separate the pitches into components and the second grating would pose an intensity.

$$I(x,y) = \frac{1}{2} + \frac{1}{2}\sin\left[2\pi(xp_x + yp_y)\right]$$

Where $p_x = p\cos\gamma$ and $p_y = p\sin\gamma$ for original pitch, p, and γ is the angle of rotation. The total transmitted intensity of the two is

$$I(x) = \left[\frac{1}{2} + \frac{1}{2}\sin(2\pi xp)\right]\left\{\frac{1}{2} + \frac{1}{2}\sin\left[2\pi(xp\cos\gamma + yp\sin\gamma)\right]\right\}$$

or

$$I(x) = \frac{1}{4}\left[1\ \sin(2\pi xp)\right]\left\{1 + \sin(2\pi px\cos\gamma)\cos(2\pi py\sin\gamma)\right.$$

$$\left. - \cos(2\pi px\cos\gamma)\sin(2\pi py\sin\gamma)\right\}$$

An example, produced by a line grating, is shown in Figure 14

Other situations are found by similar techniques of combining intensities. Results for line gratings are produced by using the Fourier expansion for the line grating and using the superposition principle to sum the resulting intensity.

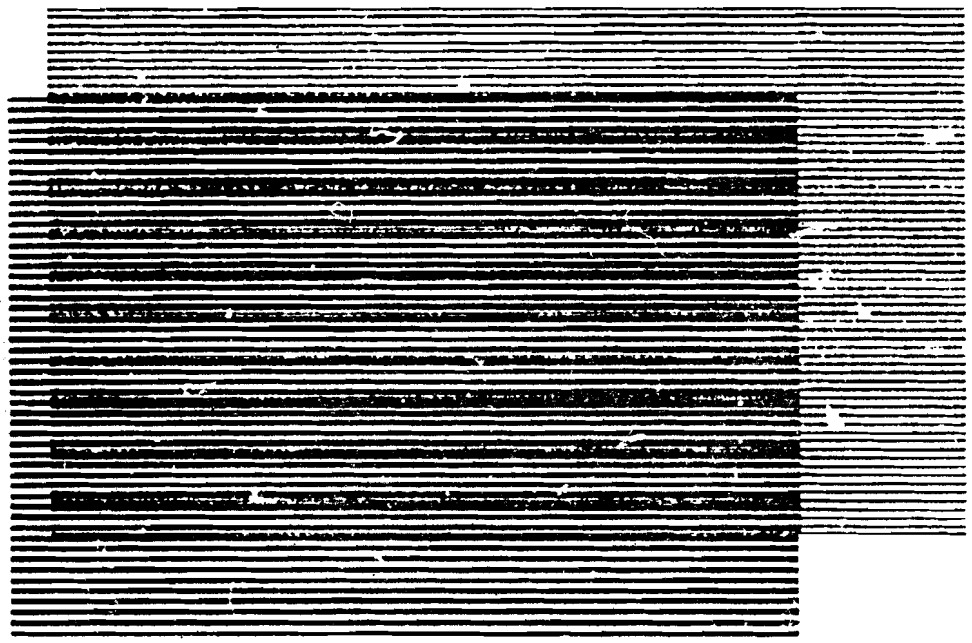

Grating 1 Grating 2

Figure 13. Moire From Two Gratings of Different Pitches

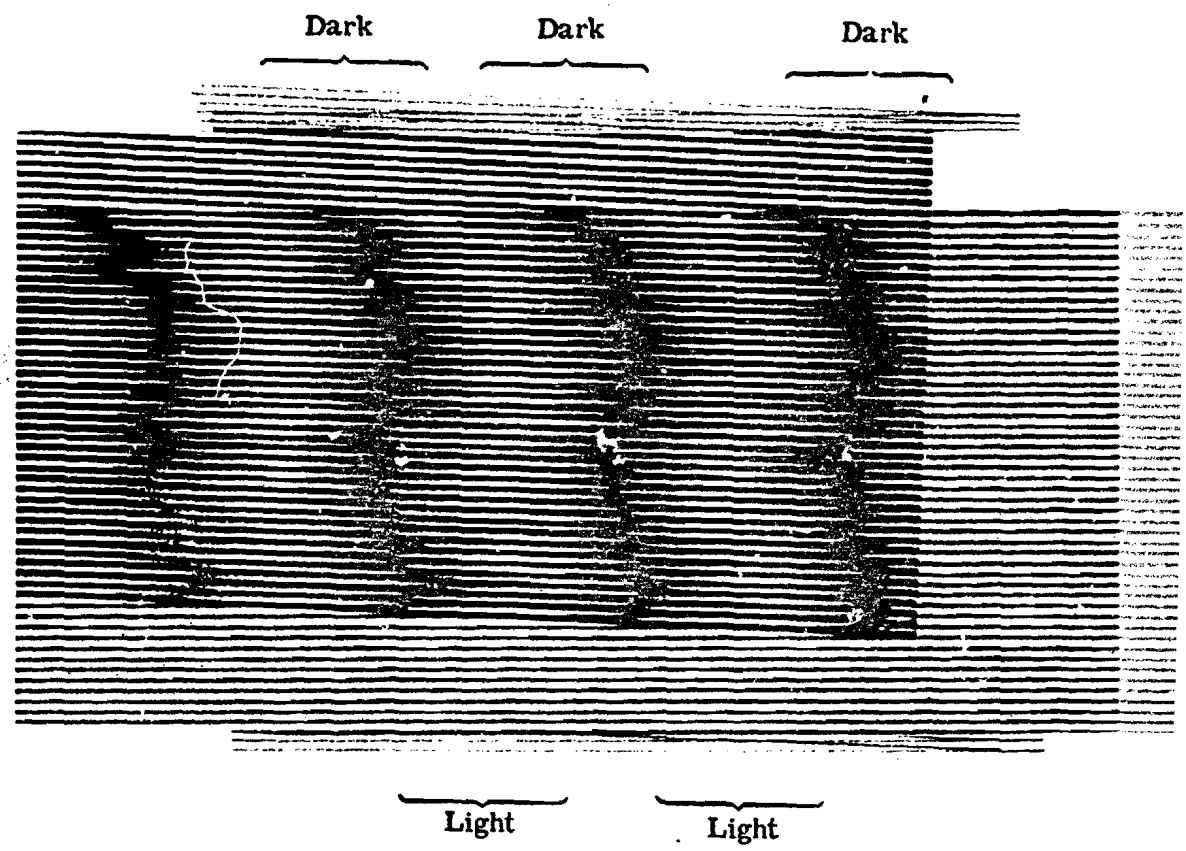

Figure 14. Moire Between Two Gratings at Angle To Each Other: Imperfections Cause Jagged Appearance in Fringes

APPENDIX D

TOPOLOGY AND DEFORMATION CONTOURING BY MOIRE FRINGES

We show here how a topological or deformation contour is generated by the comparison of grid lines. The methods of producing the grid lines are discussed elsewhere, but the analysis is essentially the same since the plane of comparison can vary if suitable imaging optics are used. This statement holds except for the double-exposure case where the scene grid and the reference grid are on the same film. For the case no separation of the images is easily obtainable, making individual grid manipulation by lenses difficult. The analysis for double-exposure contouring follows the analysis for separate grid-image analysis.

The difference between topology contours and deformation contours is that the reference for comparison for topology contours is an equally spaced grid while the deformation contour reference is a grid modulated by the surface features of the unstressed object. Since the reference grid is pitch modulated, the varying pitch must be known at some point in the scene. In order to obtain quantitative results, one option is to obtain a topology contour at the same time and determine sensitivity from considering the effect of the surface on the pitch. In addition to deformation contours, the differences in two similarly shaped objects can be compared with one as master and the other as "deformed."

To analyze contour generation by grids, consider the intensity modulation of a plane wave to be

$$I(x) = \frac{1}{2} + \frac{1}{2} \sin(2\pi\xi p_o)$$

where ξ is the position normal to the light planes. The rays of the plane wave make an angle α with the normal to the surface and a shift of the scene grid by $z(x,y) \tan \alpha$ is obtained where z is the height above a standard datum plane. Figure 15 shows the angle. The intensity on the surface is

$$I_s = K\left[\sin\left(2\pi p[x - z(x,y) \tan \alpha]\right) + 1\right]$$

where K is a factor which includes reflectivity and the original intensity divided by two and p is the original pitch p_o multiplied by $\cos \alpha$. When viewed by an observer at angle β from the surface normal, the deformation shifts the position by $z(\tan \alpha + \tan \beta)$.

The reference grid is now placed in the observation path so that it is parallel to the scene datum plane and scaled so that its pitch matches the pitch, $p = p_o(\cos \alpha)$, which is the pitch observed at the scene datum plane. For topology contouring the reference grid has intensity transmission

$$T(x) = \frac{1}{2} (1 + \sin 2\pi px)$$

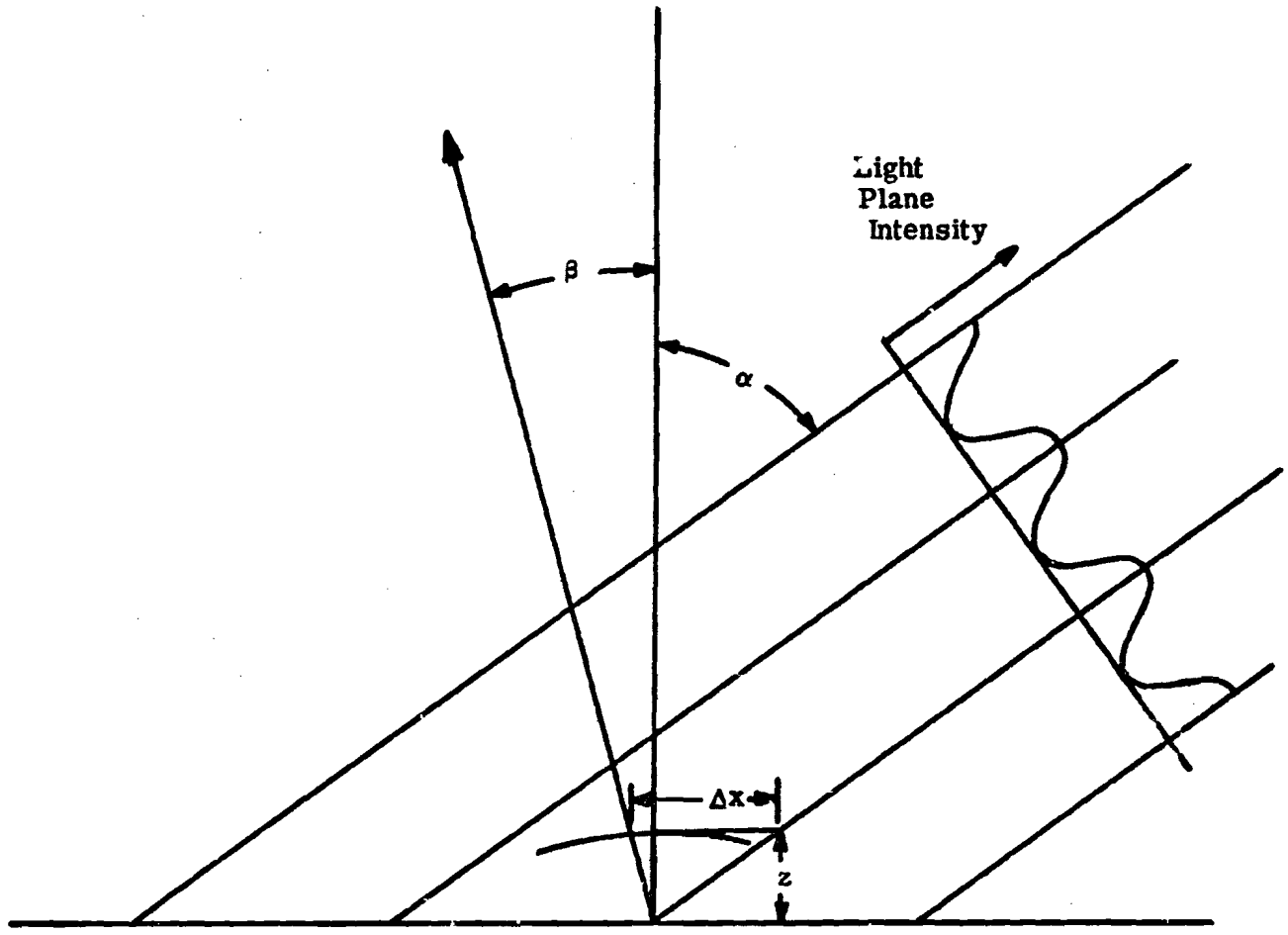

Figure 15. Geometry Showing Change in x, Δx, Due to Change in z.

The intensity behind the reference grid is

$$I = \frac{K}{2}\left(1 + \sin 2\pi px\right)\left[1 + \sin\left\{2\pi p\left(x - z \tan \alpha\right)\right\}\right]$$

substituting

$$2\pi px = a_1, b_1 = 0$$

and

$$-2\pi z \tan \alpha = b_2 = \Delta b$$

into the trigonometry identities:

$$1 + \sin\left(a_1 + b_1\right) = 1 + \sin\left(a_1 + \frac{b_1 + b_2}{2} - \frac{\Delta b}{2}\right)$$

where

$$b_1 + \Delta b = b_2$$

$$1 + \sin\left(a_1 + b_2\right) = 1 + \sin\left(a_1 + \frac{b_1 + b_2}{2} + \frac{\Delta b}{2}\right)$$

Sums gives us

$$\left[1 + \sin\left(a_1 + b_1\right)\right] + \left[1 + \sin\left(a_1 + b_2\right)\right]$$

$$= 2 + 2 \sin\left(a_1 + \frac{b_1 + b_2}{2}\right)\cos \frac{\Delta b}{2}$$

Products give us

$$\left[1 + \sin\left(a_1 + b_1\right)\right]\left[1 + \sin\left(a_1 + b_2\right)\right]$$

$$= \left[\sin\left(a_1 + \frac{b_1 + b_2}{2}\right) + \cos \frac{\Delta b}{2}\right]^2$$

We perform the multiplication to give

$$I = \left\{\sin\left[2\pi p\left(x - z\left[\tan \alpha + \tan \beta\right]\right)\right] + \cos\left(\pi z\left[\tan \alpha + \tan \beta\right]\right)\right\}^2$$

The term $\cos^2\left(\pi p z\left[\tan \alpha + \tan \beta\right]\right)$ will give moire fringes which are dependent on z and are contours of the object topology. To vary the sensitivity, we would change p_o, α or β.

This result would have the same form as the second case of Appendix C if our simplifying trigonometry had been used and fringes occur as the phase changes linearly with z.

Deformation contouring is achieved by using reference grid filter which is a recorded grid defined by the surface before deformation. The undeformed grid has intensity transmittance

$$T(x) = K\left\{1 + \sin\left[2\pi p\left(x - z_1(\tan\alpha + \tan\beta)\right)\right]\right\}$$

and the intensity from the deformed surface is

$$I_s = K'\left\{1 + \sin\left[2\pi p\left(x - z_2(\tan\alpha + \tan\beta)\right)\right]\right.$$

Multiplying these intensities gives the intensity behind the filter

$$I = KK'\left\{1 + \sin\left[2\pi p\left(x - z_1(\tan\alpha + \tan\beta)\right)\right]\right\}$$
$$\left\{1 + \sin\left[2\pi p\left(x - z_2(\tan\alpha + \tan\beta)\right)\right]\right\}$$

Using $\Delta z = z_2 - z_1$ and the trigonometry relations given earlier, we obtain

$$I = KK'\left\{\sin\left[2\pi p\left(x + \frac{(z_1 + z_2)}{2}(\tan\alpha + \tan\beta)\right.\right.\right.$$
$$\left.\left.\left. + \cos\left(\pi p\Delta z(\tan\alpha + \tan\beta)\right)\right)\right]\right\}^2$$

Thus, the moire fringes that occur here form contours of equal Δz values instead of z values.

For the double-exposure case the reference grid and the scene grid are both photographed on the same film. In this case the intensities add, and the transmittance of the developed film is

$$T = 2K\left\{1 + \sin\left(\pi p\left[2x - (z_1 + z_2)(\tan\alpha + \tan\beta)\right]\right)\right.$$
$$\left.\cos\left(\pi p\Delta z(\tan\alpha + \tan\beta)\right)\right\}$$

which is proportional to the intensity when illuminated by a plane wave. This result is similar to the result for the filter just found except no $\cos^2\left(\pi p\Delta z[\tan\alpha + \tan\beta]\right)$ term is present. Moire fringes are obtained from the single $\cos\left(\pi p\Delta z[\tan\alpha + \tan\beta]\right)$ term, but the overall sensitivity is usually limited because the viewer must be able to resolve the original generating pitch in order to see the moire. When the $\cos^2\left(\pi p\Delta z[\tan\alpha + \tan\beta]\right)$ term is present, this is not necessary and the sensitivity can be enhanced by using finer pitches for illumination of the object.

One additional use of the live fringe filter moire exists in vibration analysis. The analysis is similar to that for constant amplitude vibration measurement which requires the integration of a sinusoidal variation over a cycle

$$I_{average} = \frac{1}{P}\int_0^P I(x,y,\tau)\, d\tau$$

Replacing $z(x,y)$ by $z_o(x,y) + A(x,y)\cos(\omega\tau)$. The integral of the time-varying intensity is a first order Bessel function and the result is

$$I_{average} = K\left\{1 + \sin\left[2\pi p\left(x - z_o(\tan\alpha + \tan\beta)\right)\right]\right.$$
$$\left. J_o\left[2\pi p \tan\alpha A(x,y)\right]\right\}$$

where A(x,y) is the amplitude distribution of the vibration. The discussion of the fringes obtained is the same as for constant amplitude holographic interferometry except for the desensitization by the factor

$$\left(\frac{p \tan \alpha + \tan \beta}{\frac{1}{\lambda} (\sin \theta_1 + \sin \theta_2)} \right)$$

or approximately the ratio of the wavelength of light to the period, $\frac{1}{p}$ of the grid.

APPENDIX E

HOLOGRAPHIC CONTOURING

Dual-wavelength contouring by holography uses the same formulisms as ordinary holography except that the amplitude scattered to the plate from the scene has two components

$$A_o = O\left(e^{4\pi iz/\lambda_1} + e^{-4\pi iz/\lambda_2}\right)$$

because of the two wavelengths. The reference beam also consists of two components

$$A_R = R\left(e^{-2\pi ix\sin\theta/\lambda_1} + e^{-2\pi ix\sin\theta/\lambda_2}\right)$$

where θ is the offset angle.

The amplitudes add at the plate; and, when developed, the amplitude transmittivity is proportional to the intensity

$$t = C\left(A_oA_o^* + A_RA_R^* + A_oA_R^* + A_RA_o^*\right)$$

The term of interest is the one with the object amplitude in it, and upon applying the reconstruction beam we obtain an amplitude

$$A_c = Ce^{-2\pi ix\sin\theta/\lambda_c}$$

We obtain the amplitude behind the plate which is moving close to the original object beam direction. This amplitude is

$$A_p = CA_cA_RA_o$$

Now we substitute to find the amplitude in terms of the original variable

$$A_p = Ce^{-2\pi ix\sin\theta/\lambda_c}R\left(e^{+2\pi ix\sin\theta/\lambda_1} + e^{+2\pi ix\sin\theta/\lambda_2}\right)$$
$$\times\ 0\left(e^{-4\pi iz/\lambda_1} + e^{-4\pi iz/\lambda_2}\right)$$

Note that there is a problem in reconstruction since both λ_1 and λ_2 cannot be eliminated with a simple reference beam. The difference in wavelength gives two images which leave it slightly different directions because of the wavelength differences. For the case where both wavelengths are available for reconstruction, such as for the argon-ion laser, there are proper terms in the object beam directions. This term is

$$A_t = C\left[e^{-2\pi i\cdot 2z/\lambda_1} + e^{-2\pi i\cdot 2z/\lambda_2}\right]$$

or

$$A_t = 2C\left[1 + \cos\left(4\pi z\left(\frac{1}{\lambda_1} - \frac{1}{\lambda_2}\right)\right)\right]$$

which has bright fringes when

$$2z\left[\frac{1}{\lambda_1} - \frac{1}{\lambda_2}\right] = N$$

where N = 0, 1, 2, ... Solving for the depth for a bright fringe, we find

$$z = \frac{N\lambda_1\lambda_2}{2|\lambda_2 - \lambda_1|}$$

Other schemes are possible for application at reconstruction time to reduce the effect of the reconstruction wavelength differences in dual-wavelength contouring. One can use a diffraction grating to input the reference and reconstruction beam into the hologram plate. Since sin θ/λ is a constant for any wavelength, the different wavelength beams make different angles with the plate and the problem is eliminated. Also, the hologram should be an image hologram which has the image of the scene located close to the hologram plate. This reduces the reconstruction problem by minimizing z.

APPENDIX F

PROJECTED-MOIRE GRID SENSITIVITY

The sensitivity of projected moire grids for the detection of deformations depends on the locations of the observer, the dual sources, and the object point that is to have its deformation measured. Also, the orientation of the projected fringes with these positions is to be considered. The diagram of Figure 15 shows the simplified case where we are viewing the scene from the normal direction to the plane formed by the observer, the center of the dual sources, and the object point. The light planes are normal to that plane also and their intensities are indicated by the plot along the perpendicular to their path. The deformed surface intercepts the light planes and the shift of the light planes is a measure of the deformation. This shift is detected by comparison with a record of the light plane interception with the reference surface by a moire comparison. The moire results in a new picture of the surface with a superposition of fringes which define the locus of equal deformation regions. This fringe production has been discussed in Appendix D. Coordinate transformations are necessary to convert to other systems, e.g., the prime mover system. Since the contour map gives a whole field, this transformation can be handled after the collection of data without shifting errors by choosing the desired points in the scene for analysis with respect to the desired coordinate system.

We may find the relationship between the deformation, δ, the grid spacing L_o and the experimental geometry by considering Figure 16. Here the light planes are shown striking a surface in the coordinate system whose center is shown. The unit vectors, $\hat{v}$, $\hat{s}$, $\hat{n}$, and $\hat{t}$ define the directions from the point to be analyzed, (x, y, z), toward the viewer, along the perpendicular between light planes, along the normal to the surface and toward the point between the dual sources, respectively.

The distance along the viewing vector $\hat{v}$ between light planes is the deformation Λ which produces a full 2π phase change in the fringe at the point. This distance is related to the grid spacing by

$$\delta = L/(\hat{s} \cdot \hat{v})$$

where $\hat{s} \cdot \hat{v} = \cos\phi$. The normal component of this motion is the deformation of interest so

$$\Lambda = \delta_1 \cos\phi \text{ or in vector terms}$$

$$\Lambda = L[(\hat{v} \cdot \hat{n})/(\hat{s} \cdot \hat{v})]$$

We must now determine these angles in terms of experimental locations. The angle between the normal and the line to the observer is given by

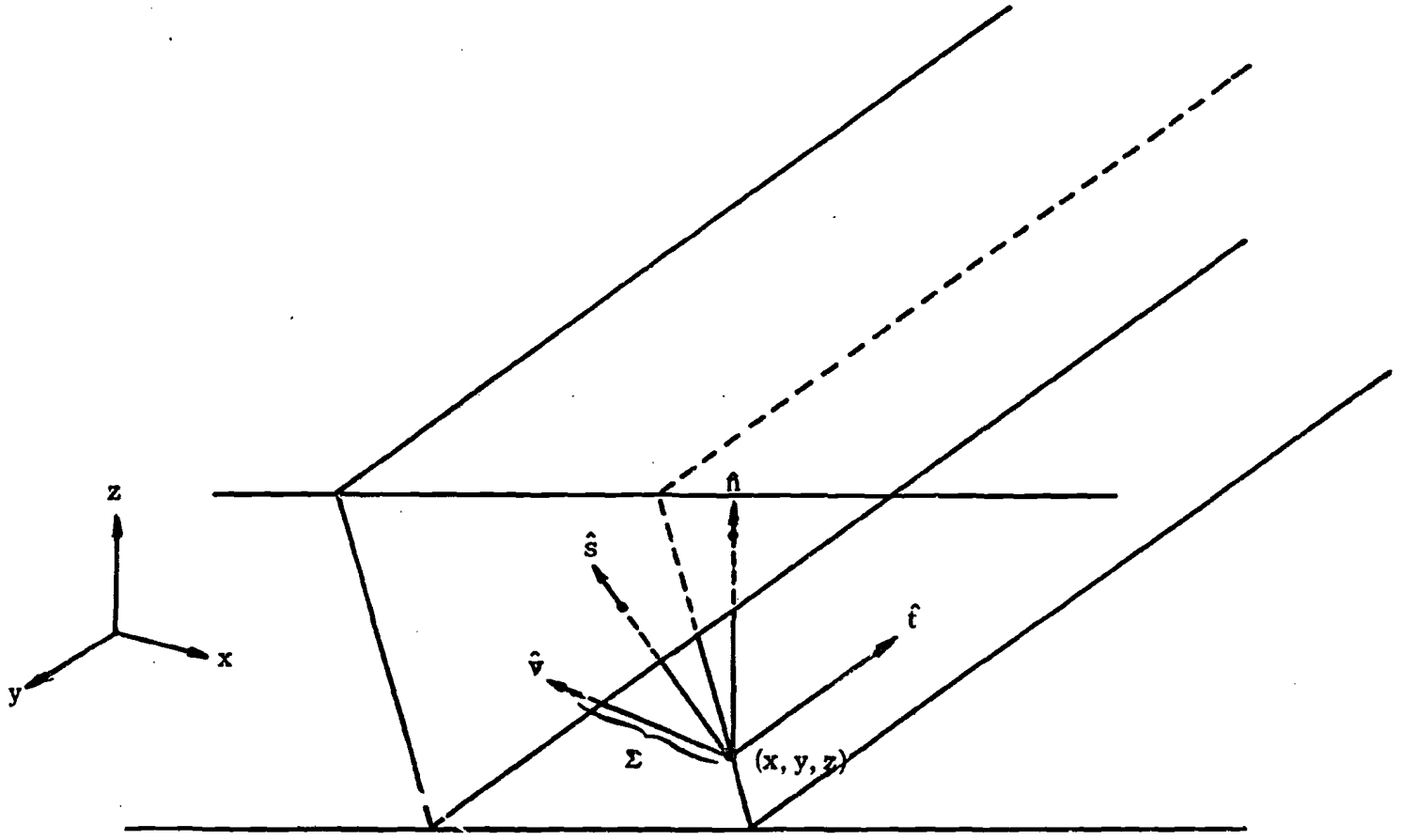

Figure 16. Three-Dimensional Moire Analysis Geometry.

$$\beta = \tan^{-1}\left\{\frac{\sqrt{(V_x - x)^2 + (V_y - y)^2}}{(V_z - z)}\right\}$$

where V is the observer position. Likewise the angle between the normal and the line to the midpoint of a line between the two sources is

$$\alpha = \tan^{-1}\left\{\frac{\sqrt{(T_x - x)^2 + (T_y - y)^2}}{(T_z - z)}\right\}$$

where T is the midpoint source position.

The angle α is required in determining the deformation in order to find the angle between the surface normal and the perpendicular to the light planes. We use the spherical angle equation

$$\text{Cos } C = \text{Cos } A \cos A' + \sin A \sin A' \cos(B' - B)$$

where A, A', B, B', and C are shown in Figure 18. C is the angle to be found. The diagram in Figure 19 shows the relationship between the light planes and the source and if the axis is taken to be the line to the source midpoint substitutions

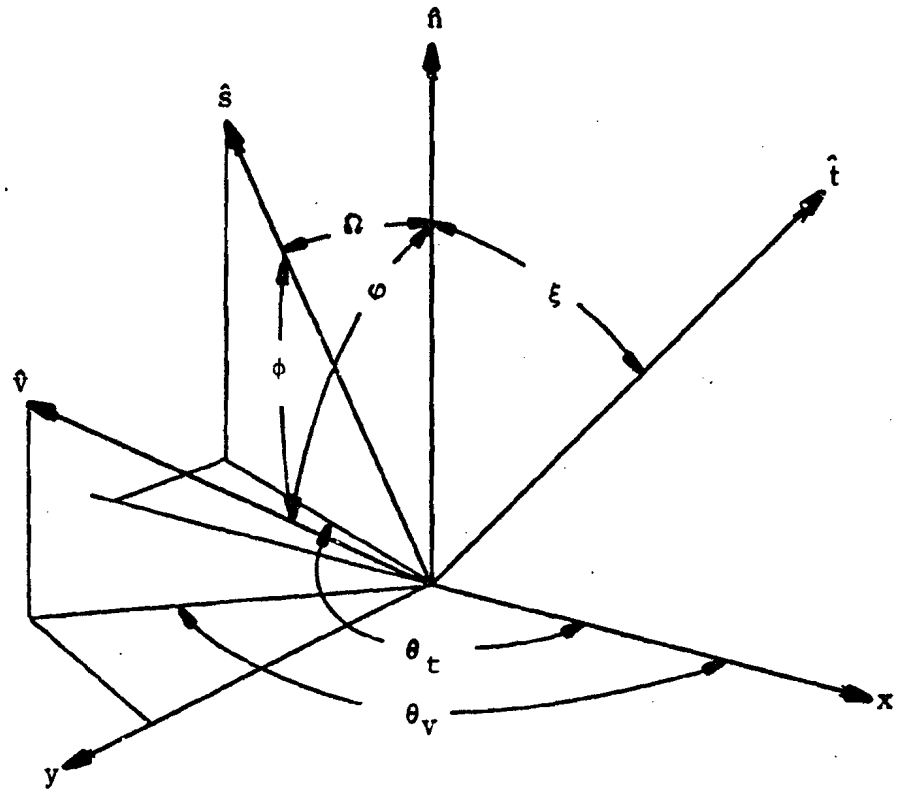

Figure 17. Moire Analysis Angle Detail.

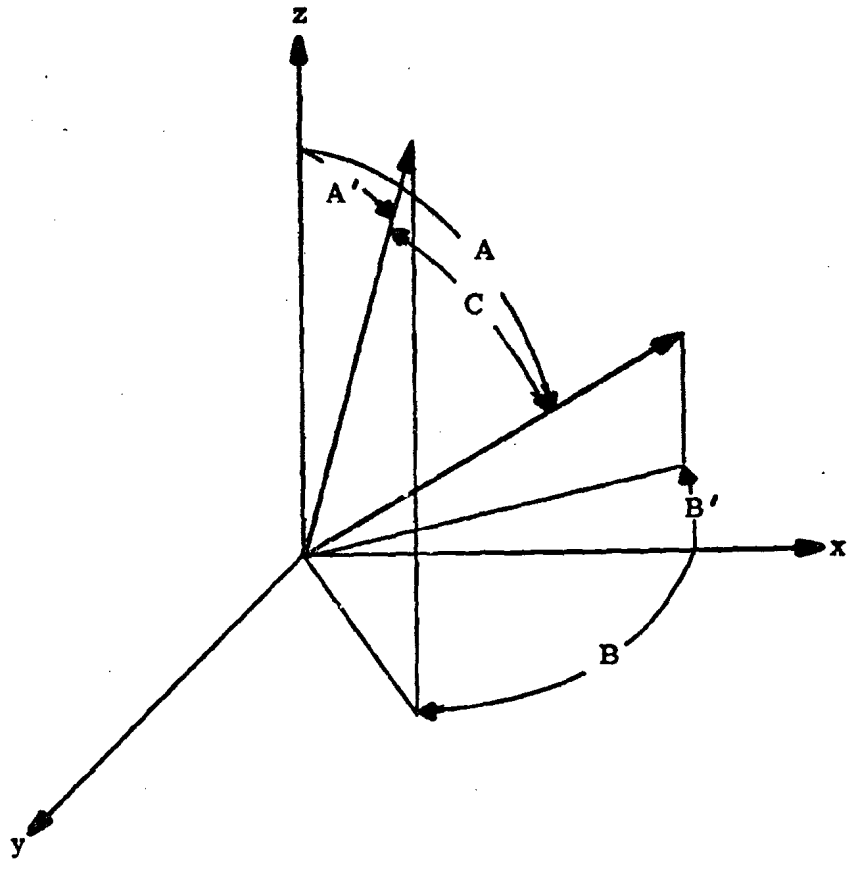

Figure 18. Spherical Angles for Finding Angle between Two Vectors.

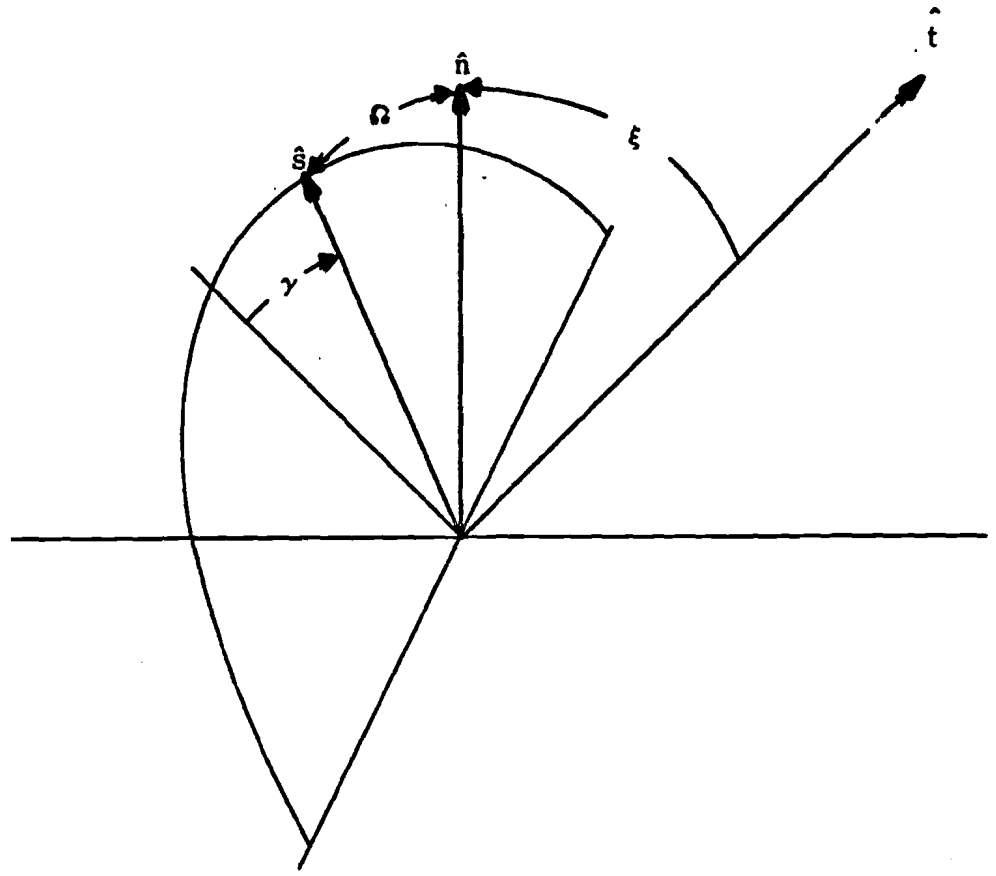

Figure 19. Geometry to Determine Angles.

$$A = \alpha,\ A' = 90^{\circ}$$
$$B = 0,\ B' = \gamma$$
$$C = \Omega$$
$$\Omega = \cos^{-1}(\sin\alpha\cos\gamma)$$

Now back to Figure 17 because the normal as the axis to find the angle between the line to the viewer and the perpendicular between the light planes by substituting

$$A = \Omega,\ A' = \beta$$
$$B = \theta_s,\ B' = \theta_v$$
$$C = \phi$$

to get $\cos\phi = \cos\Omega + \sin\beta\cos(\theta_t - \theta_v)$ where $\theta_t = \tan^{-1}\left(\frac{T_y}{T_x}\right)$ and

$$\theta_v = \tan^{-1}\left(\frac{V_y}{V_x}\right)$$

Thus, the angles β and ϕ have been found and by substitution the deformation can be related to the phase change in the moire. The deformation in general is not a 2π change so for a change in order, ΔO, the normal component of the deformation is given by

$$\Lambda = \Delta O\left[L\ \frac{(\hat{n}\cdot\hat{v})}{(\hat{s}\cdot\hat{v})}\right]$$

BIBLIOGRAPHY

OPTICS

Born, M., and Wolf, E., Principles of Optics, Pergamon Press, 1970.

Jenkins, F. A., and White, H. E., Fundamentals of Optics, McGraw-Hill Company, New York, 1957.

Johnson, B. K., Optics and Optical Instruments, Dover Publications, Inc., New York.

Murphy, C. G., and Alpert, S. S., Dependence of Refractive Index Temperature Coefficient on the Thermal Expansivity of Liquids, American Journal of Physics, Vol. 39/7, USA, 1971.

RCA, Electro-Optics Handbook, RCA Commercial Engineering, New Jersey.

Sears, F. W., Optics, Addison-Wesley Company, Inc., Massachusetts.

HOLOGRAPHY, GENERAL

Collier, R. J.; Burckhardt, C.B.; and Lin, L. H., Optical Holography, Academic Press, New York, 1971.

DeVelis, J. B., and Reynolds, G.O., Theory and Applications of Holography, Addison-Wesley, Massachusetts.

Hodgman, C. D.. ed., Standard Mathematical Tables, Chemical Rubber Publishing Company, Ohio.

Jackson, J. D., Classical Electrodynamics, John Wiley & Sons, Inc., New York.

Jahnke, E., and Emde, F., Tables of Functions with Formulae and Curves, Dover Publications, New York.

Murphy, C. G., and Landry, M. J., Holography in a Modern Laboratory, SC-DC-72-1230, Sandia Laboratories, Albuquerque, N. M., 1972.

Proceedings of the Engineering Applications of Holography Symposium Advanced Research Projects Agency, and TRW Systems Group, Los Angeles, California, 1972. (Available from SPIE, Redondo Beach, California).

Smith, H. M., Principles of Holography, Wiley-Interscience, John Wiley & Sons, Inc., New York.

Thompson, B. J., and DeVelis, J. B., ed., Developments in Holography, Seminar Proceedings, Society of Photo-Optical Instrumentation Engineers, Vol. 25, 1971.

HOLOGRAPHY, CONTOURING

Gara, A. D.; Majkowski, R. F.; and Stapleton, T. T., "Holographic Systems for Automatic Surface Mapping," Applied Optics, Vol. 12 No. 9, 1973.

Hildebrand, B. P., and Haines, K. A., "Multiple-Wavelength and Multiple-Source Holography Applied to Contour Generation," Journal of the Optical Society of America, Vol. 57, 1967.

Varner, J. R., Holographic Contouring: Alternatives and Applications, Developments in Holography, (cited above).

HOLOGRAPHY, INTERFEROMETRY

Aleksandrov, E. B., and Bonch-Bruevich, A. M., "Investigation of Surface Strains by the Hologram Technique," Soviet Physics-Technical Physics, Vol. 12, No. 258, 1967.

Ashton, R. A.; Slovus, D.; and Gerritsen, H. J., "Interferometric Holography Applied to Elastic Stress and Surface Corrosion," Applied Optics, Vol. 10, No. 440, 1971.

Burchett, O. J. and Irwin, J. L., "Using Laser Holography for Nondestructive Testing," Mechanical Engineering, Vol. 93, No. 27, 1971.

Ennos, A. E., "Measurements of In-Plane Surface Strain by Hologram," Journal of Scientific Instruments, (J. of Phys. E.), Ser. 2, 1, 731, 1968.

Haines, K. A., and Hildebrand, B. D., "Surface Deformation Measurement Using the Wave Front Reconstruction Technique," Applied Optics, Vol. 5, No. 595, 1966.

Hansche, B. D., "The Application of Holometry to Deformation Analysis of Spheres," SC-DR-71-0530, Sandia Laboratories, Albuquerque, N. M., 1971.

Hansche, B. D., and Murphy, C. G., "Strain Measurements by Holometry," ISA Transactions, Vol. 11:1, 1972.

Hansche, B. D., and Murphy, C. G., "Holographic Analysis from a Single View," Applied Optics, (In Press).

Murphy, C. G.; Burchett, O. J.; and Matthews, C. W., "Holometric Deformation Measurement on Carbon Carbon Biaxial Test Specimens," Proceedings Engineering Applications of Holography, Society of Photo-Optical Instrumentation Engineers, Redondo Beach, California, 1972.

Murphy, C. G.; Burchett, O. J.; and Matthews, C. W., "Flaw Detection Sensitivity of Holographic Interferometry on Cylinders Under Hoop Stress," Proceedings of the Technical Program Electro-Optical Systems Design Conference, Industrial and Scientific Conference Management, Chicago, 1971.

Murphy, C. G.; Morrison, D. M.; Crosley, W. C., and Wise, C. M., "Mini-Computer Image Storage for Holographic Interferometry Analysis," 16th Annual SPIE Seminar, 1972.

Murphy, C. G.; Hansche, B. D.; and Burchett, O. J., "Prediction of Holographic Interferometry Experiment Results," 13th Annual Fracture and Flaws Symposium, Albuquerque, New Mexico, March 1973.

Powell, R. L., and Stetson, K. A., "Interferometric Hologram Evaluation and Real-Time Vibration Analysis of Diffuse Objects," Journal of the Optical Society of America, Vol. 55, No. 1593, 1965.

Sampson, R. C., "Holographic-Interferometry Applications in Experimental Mechanics," Experimental Mechanics, Vol. 10, No. 313, 1970.

Sollid, J. E., "Holographic Interferometry Applied to Measurements of Small Static Displacements of Diffusely Reflecting Surfaces," Applied Optics, Vol. 5, No. 595, 1966.

Stetson, K. A., and Powell, R. L., "Hologram Interferometry," Journal of the Optical Society of America, Vol. 56, No. 1161, 1966.

Wells, D. R., "NDT of Sandwich Structures by Holographic Interferometry," Materials Evaluation, Vol. 27, No. 225, 1969.

Wuerker, R. F., "Holographic Interferometry," Developments in Holography, SPIE Seminar Proceedings, Vol. 25, No. 225, 1971.

MOIRE

Brooks, R. E., and Heflinger, L. O., "Moire Gauging Using Optical Interference Patterns," Applied Optics, Vol. 8, No. 5, 1969.

Der Hovanesian, J.; Haskell, R. E.; and Powell, R. L., "Use of a Projected-Ruling Moire Method for Vibration and Deflection Measurements of Three-Dimensional Structures," Engineering Applications of Holography (cited above).

Duffy, D. E., "Moire Gauging of In-Plane Displacement Using Double Aperture Imaging," Applied Optics, Vol. 11, No. 8, 1972.

Jaerisch, W., and Makosch, G., "Optical Contour Mapping of Surfaces," Applied Optics, Vol. 12, No. 7, 1973.

Meadows, D. M.; Johnson, W. O.; and Allen, J. B., "Generation of Surface Contours by Moire Patterns," Applied Optics, Vol. 9, No. 4, 1970.

Pryor, T. R.; Hageniers, O. L.; and North, W. P. T., "Diffractographic Moire Technique Illustrated by Determination of Beam Deflections," Journal of Strain Analysis, Vol. 8, No. 1, 1973.

Takasaki, H., "Moire Topography," Applied Optics, Vol. 9, No. 6, 1970.

Takasaki, H., "Moire Topography," Applied Optics, Vol. 12, No. 4, 1973.

Theocaris, P. S., Moire Fringes in Strain Analysis, Pergamon Press.

FOURIER OPTICS

Bracewell, R., The Fourier Transform and Its Applications, McGraw-Hill Company, New York.

Goodman, J. W., Introduction to Fourier Optics, McGraw-Hill Company, New York.

Shulman, A. R., Optical Data Processing, John Wiley & Sons, Inc., New York.

LASERS

Lengyel, B. A., Lasers, Wiley-Interscience, John Wiley & Sons, Inc., New York.

Pressley, R. J., Handbook of Lasers with Selected Data on Optical Technology, The Chemical Rubber Company, Ohio.

Yariv, A., Introduction to Optical Electronics, Holt, Rinehart and Winston, Inc., New York.